



Dual roles of HSP70 chaperone HSPA1 in quality control of nascent and newly synthesized proteins

Guiyou Tian¹ , Cheng Hu¹ , Yun Yun¹ , Wensheng Yang², Wolfgang Dubiel^{1,3}, Yabin Cheng^{1,4,*} & Dieter A Wolf^{1,4,**}

Abstract

Exposure to heat stress triggers a well-defined acute response marked by HSF1-dependent transcriptional upregulation of heat shock proteins. Cells allowed to recover acquire thermotolerance, but this adaptation is poorly understood. By quantitative proteomics, we discovered selective upregulation of HSP70-family chaperone HSPA1 and its co-factors, HSPH1 and DNAJB1, in MCF7 breast cancer cells acquiring thermotolerance. HSPA1 was found to have dual function during heat stress response: (i) During acute stress, it promotes the recruitment of the 26S proteasome to translating ribosomes, thus poisoning cells for rapid protein degradation and resumption of protein synthesis upon recovery; (ii) during thermotolerance, HSPA1 together with HSPH1 maintains ubiquitylated nascent/newly synthesized proteins in a soluble state required for their efficient proteasomal clearance. Consistently, deletion of HSPH1 impedes thermotolerance and esophageal tumor growth in mice, thus providing a potential explanation for the poor prognosis of digestive tract cancers with high HSPH1 and nominating HSPH1 as a cancer drug target. We propose dual roles of HSPA1 either alone or in complex with HSPH1 and DNAJB1 in promoting quality control of nascent/newly synthesized proteins and cellular thermotolerance.

Keywords co-translational protein quality control; esophageal cancer; heat shock protein 70; stress response; ubiquitin-proteasome system

Subject Categories Post-translational Modifications & Proteolysis; Translation & Protein Quality

DOI 10.15252/embj.2020106183 | Received 9 July 2020 | Revised 6 April 2021 | Accepted 15 April 2021 | Published online 19 May 2021

The EMBO Journal (2021) 40: e106183

Introduction

In warm-blooded species, proteins are continuously exposed to damaging influences that lead to rapid protein denaturation, frequently exacerbated by chronic states of infection, exposure to

toxicants, mal- and overnutrition, or inflammation. A defining feature of misfolded proteins is their tendency to aggregate. Such aggregates are implicated in the pathogenesis of a wide range of human disorders, including neurodegeneration and type II diabetes (Buchberger *et al*, 2010; Hartl *et al*, 2011; Amm *et al*, 2014; Ciechanover & Kwon, 2017). On the flip side, the cytotoxicity of protein aggregates is being exploited for cancer therapy, for example, by administration of proteasome inhibitors (Chatterjee & Burns, 2017).

The ubiquity and deleterious consequences of protein misfolding necessitate stringent quality control mechanisms. Chief contributor to protein quality control is a large network of chaperones, factors that assist in the folding or disaggregation of proteins (Frydman, 2001; Hartl & Hayer-Hartl, 2009; Kramer *et al*, 2009). If the load of misfolded proteins exceeds the folding capacity of chaperones, denatured proteins or the resulting aggregates are cleared by selective degradation. One of the best-studied such pathways is the degradation of proteins that fail to fold correctly in the endoplasmic reticulum (ER) (Stolz & Wolf, 2010). Such terminally misfolded proteins are retro-translocated into the cytoplasm and cleared by ubiquitin-proteasome-dependent ER-associated degradation (ERAD) and presumably autophagy.

Cells also rapidly degrade abnormal proteins that result from errors in translation and/or unsuccessful post-synthetic folding. Peri-translational protein quality control is executed by a complex network of chaperones organized in the vicinity of the ribosome (Pechmann *et al*, 2013; Döring *et al*, 2017; Thommen *et al*, 2017; Kramer *et al*, 2018; Joazeiro, 2019). Nascent polypeptide-associated complex (NAC) is a heterodimeric complex that binds in and around the ribosome exit tunnel (Gamerding *et al*, 2019). The ribosome-associated complex (RAC) is composed of a specialized HSP70 protein (HSPA14) and a cognate HSP40 J domain protein (DNAJ2) (Hundley *et al*, 2005; Otto *et al*, 2005; Jaiswal *et al*, 2011). This complex recruits other HSP70 chaperones—Ssb in yeast and HSPA1 in mammalian cells—to ribosome-bound nascent peptides (Jaiswal *et al*, 2011). Yeast Ssb chaperones assist co-translational protein folding, facilitate rapid protein synthesis, and support efficient membrane targeting (Willmund *et al*, 2013; Döring *et al*, 2017; Stein *et al*, 2019).

1 School of Pharmaceutical Sciences, State Key Laboratory of Cellular Stress Biology, Fujian Provincial Key Laboratory of Innovative Drug Target Research, Xiamen University, Xiamen, China

2 Department of Pathology, Chenggong Hospital of Xiamen University, Xiamen, China

3 Institute of Experimental Internal Medicine, Medical Faculty, Otto von Guericke University, Magdeburg, Germany

4 Fujian Provincial Key Laboratory of Innovative Drug Target Research, Xiamen University, Xiamen, China

*Corresponding author. Tel: +86 592 2181852; E-mail: chengyb@xmu.edu.cn

**Corresponding author. Tel: +86 592 2181852; E-mail: dwolf@xmu.edu.cn

Proteins that cannot attain a stably folded conformation during or shortly after synthesis are thought to be degraded by the ubiquitin-proteasome system. For example, ~15% of nascent polypeptides are ubiquitylated by E3 ligases such as CCR4/Not, Listerin, UBR4/5, and HUWE1 (Bengtson & Joazeiro, 2010; Duttler *et al.*, 2013; Wang *et al.*, 2013; Yau *et al.*, 2017), followed by degradation by the 26S proteasome (Liao *et al.*, 1998; Sato *et al.*, 1998; Schubert *et al.*, 2000; Turner & Varshavsky, 2000; Chuang *et al.*, 2005; Ha *et al.*, 2016). Considering the preferential sensitivity of nascent and newly synthesized proteins to stress-induced ubiquitylation and proteasomal degradation (Medicherla & Goldberg, 2008; Kim *et al.*, 2011; Yau *et al.*, 2017), the fraction of such peri-translationally degraded proteins may drastically increase under proteotoxic stress conditions (Wang *et al.*, 2013; Yau *et al.*, 2017).

Although it is well established that chaperones and the proteasome are involved in the quality control of newly synthesized proteins, mechanisms coupling co-translational folding/misfolding with degradation remain poorly defined. Studying an adaptive thermotolerance paradigm, we defined new dual roles of HSP70 family member HSPA1 in the quality control of nascent/newly synthesized proteins.

Results

MCF7 cells rendered thermotolerant are resistant to heat stress-induced inhibition of protein synthesis

To study dynamic responses to heat stress, we subjected MCF7 cells to a scheme of temperature changes inducing thermotolerance. Cells were exposed to 42°C for 1 h, followed by recovery at 37°C for 4 h (Fig 1A). The initial heat treatment of heat stress naïve MCF7 cells (42°C for 1 h) did not induce cell detachment from tissue culture plates or overt cell death (Fig EV1A). However, challenge of heat stress naïve MCF7 cells with exposure to 45°C for prolonged periods led to rapid loss of viability, indicating their sensitivity to heat stress. In contrast, MCF7 cells that underwent the thermotolerance-inducing scheme showed markedly improved survival at 45°C (Fig 1B). Throughout this manuscript, MCF7 cells rendered adaptively thermotolerant through this temperature shifting procedure are referred to as MCF7^{aTT} cells.

Heat stress is known to rapidly inhibit protein synthesis at the level of translation initiation and elongation (Shalgi *et al.*, 2013). Using sucrose density gradient centrifugation, we found a highly significant reduction in the polysome to monosome ratio upon exposure of naïve MCF7 cells to heat stress at 42°C for 1 h (Fig 1C) which indicated inhibition of protein synthesis. In contrast, protein synthesis was partly resistant to heat stress in MCF7^{aTT} cells (Fig 1C). Thus, the heat stress and recovery paradigm developed here activates an adaptive program that prevents heat-induced translational arrest and induces thermotolerance of MCF7 cells.

Proteomic response to heat stress: Thermotolerant cells selectively upregulate HSPA1 and its co-chaperones DNAJB1 and HSPH1

To obtain unbiased insight into the thermotolerance program, we performed SILAC-based quantitative proteomics of MCF7 cells

exposed to 42°C and allowed to recover at 37°C, followed by re-challenge of adapted cells with heat stress. Altogether, 1,554 proteins common to all three conditions were quantified, and their relative abundance was clustered by an unsupervised self-organizing map algorithm. As expected, heat stress had a profound impact on protein levels of naïve MCF7 cells, leading to the up- and down-regulation of hundreds of proteins (Fig 2A). Some of the changes persisted during recovery from heat stress, whereas others were transient with pre-stress levels being largely restored upon recovery (Fig 2A). A substantial number of proteins were also induced or repressed selectively in recovered, heat adapted MCF7^{aTT} cells, indicating that MCF7^{aTT} cells had adopted a new steady state that differed from that of naïve MCF7 cells (Fig 2A). Re-challenge of MCF7^{aTT} cells with heat stress again led to a pronounced proteomic response, although this response markedly differed from that of naïve MCF7 cells (Fig 2A). The proteomic profiles indicated that acquisition of thermotolerance coincided with the adoption of a new steady state that is not mute to heat stress but rather elicits a distinct response pattern.

To characterize this pattern, we focused on those proteins that showed the most robust changes under the various treatments. We performed three comparisons: (i) naïve MCF7 cells exposed to heat stress at 42°C versus naïve MCF7 cells maintained at 37°C (ratio of 42°C/37°C; acute heat stress); (ii) MCF7^{aTT} cells derived after recovery from heat stress versus naïve MCF7 cells heat-stressed at 42°C (aTT/42°C); (iii) thermotolerant MCF7^{aTT} cells re-challenged with exposure to heat at 42°C versus MCF7^{aTT} cells (aTT 42°C/aTT). Unlike in Fig 2A, in this scheme, protein expression changes in response to each of the sequential treatments were not measured against the single initial unperturbed reference (i.e., naïve MCF7 cells at 37°C). Rather, each perturbation was quantified relative to its preceding condition during the sequential treatment schedule. This allowed us to pinpoint heat stress-induced deviations from the newly acquired steady state of MCF7^{aTT} cells (Fig 2B).

As expected, protein ratios in all three comparisons showed a near normal distribution centered around a mean ratio of 1.0 (Fig 2B). In each comparison, we identified ~100 proteins that were upregulated and an approximately equal number that were downregulated (Z score > 1 , < -1 , Fig 2B). Interrogating these protein sets for enrichment of Gene Ontology functional terms, we found that the set of proteins upregulated in naïve MCF7 cells upon acute heat stress was enriched for mRNA splicing and mitochondrial protein import, while the set of downregulated proteins was enriched for terms related to protein synthesis (Fig 2C). The latter finding is in agreement with rapid inhibition of protein synthesis in response to heat stress (Fig 1C). The data are also consistent with our previous observation of increased production of mitochondrial proteins in response to exogenous stress, possibly as a compensatory response to stress-induced inhibition of mitochondrial respiration (Rico-Bautista *et al.*, 2013).

As cells recovered from heat stress, they upregulated functions related to protein synthesis, heat shock response, and autophagy, while downregulating other protein quality control functions related to ER stress and translational fidelity. This response may signify recovery from the acute stress and attainment of a new, adapted steady state marked by a persistent upregulation of stress defense mechanisms such as autophagy. This proteomic signature is consistent with the recovery of protein synthesis we observed in MCF7^{aTT}

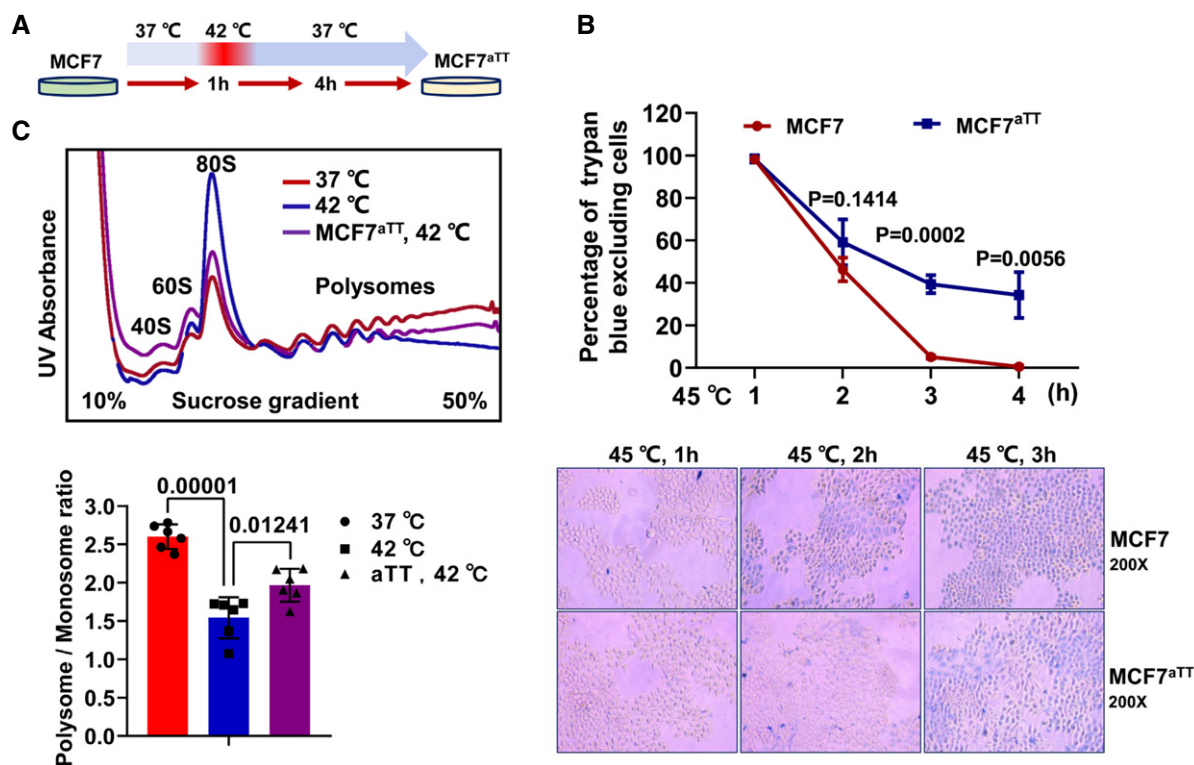


Figure 1. Heat shock and recovery leading to thermotolerance.

A Schematic diagram of the temperature shift procedure to render MCF7 cells into thermoresistant MCF7^{aTT} cells.

B Sensitivity of MCF7 and MCF7^{aTT} cells to heat shock at 45°C as determined by trypan blue staining. The graph shows means \pm SD, $n = 3$. Numbers indicate P values.

C Lysate of MCF7 and MCF7^{aTT} cells (rendered thermoresistant through the protocol described in A) were separated by sucrose density gradient centrifugation, and P/M ratios were determined by integration of monosomal and polysomal peak areas (bar graph, mean P/M ratios \pm SD, $n = 6$). Numbers above bars indicate P values calculated with the two-stage linear step-up procedure of Benjamini, Krieger, and Yekutieli.

cells (Fig 1C) which was also seen in another recent study (Määttä *et al*, 2020).

To a re-challenge with acute heat stress, thermotolerant MCF7^{aTT} cells reacted with marked upregulation of the mitochondrial respiration chain, oxidative stress defense, and co-translational protein quality control, responses that were not observed with naïve MCF7 cells (Fig 2C). The proteomic data strongly suggested that the newly acquired, adapted steady state of thermotolerant MCF7^{aTT} cells affords an improved response to acute heat stress due to augmented energy production, stress defense, and protein quality control mechanisms.

The above conclusion prompted us to interrogate the dynamics of individual chaperones during the heat stress and recovery time course. Many chaperones from the HSP10, 20, 40, 60, 70, and 90 families were induced by heat shock for 1–4 h (Fig 2D). However, among HSP70 family members, only HSPA1 remained elevated and was, in fact, hyper-induced during recovery. Remarkably, two other proteins known to cooperate with HSPA1 as part of a protein disaggregase complex (Shorter, 2011), the HSP40 family member DNAJB1 and HSPH1, the cognate nucleotide exchange factor (NEF) of HSPA1, were also hyper-induced during the recovery phase (Fig 2D). Other HSP70 NEFs, including HSPH2 and HSPH3, were downregulated during acute heat stress with basal levels being restored during recovery (Fig 2D). Selective induction and robust persistence of HSPH1 and HSPA1 during recovery was confirmed by

immunoblot analysis, suggesting a unique involvement of these chaperones in thermotolerance (Fig EV1B). Calculating normalized spectral abundance factors for absolute protein amounts revealed HSPA1 as the most abundant HSP70 family member in MCF7^{aTT} cells (Fig EV1C). Likewise, DNAJB1 and HSPH1 were the most abundant HSP40 and NEFs in thermotolerant cells.

To determine whether HSPA1 upregulation mediates thermotolerance, we employed the HSP70 inhibitor VER-155008. Although the inhibitor had no effect on the viability of MCF7^{aTT} cells on its own, it potently reversed the thermotolerance of MCF7^{aTT} cells (Figs 2E and EV1D). Taken together, the proteomic and cell viability data suggest that selective induction of HSPA1 and its co-chaperones HSPH1 and DNAJB1 mediates thermotolerance.

Thermotolerant cells are protected from the aggregation of ubiquitylated proteins through increased HSP70 activity

Given the known activity of a complex of HSPA1, HSPH1, and DNAJB1 (HHD) as well as related HSP70-HSPH-J domain protein complexes in protein disaggregation and reactivation (Shorter, 2011; Nillegoda *et al*, 2015; Faust *et al*, 2020; Wentink *et al*, 2020), we sought to test whether naïve MCF7 and thermotolerant MCF7^{aTT} cells differed in the heat-induced accumulation of detergent-insoluble protein aggregates. Total cell lysates were separated into

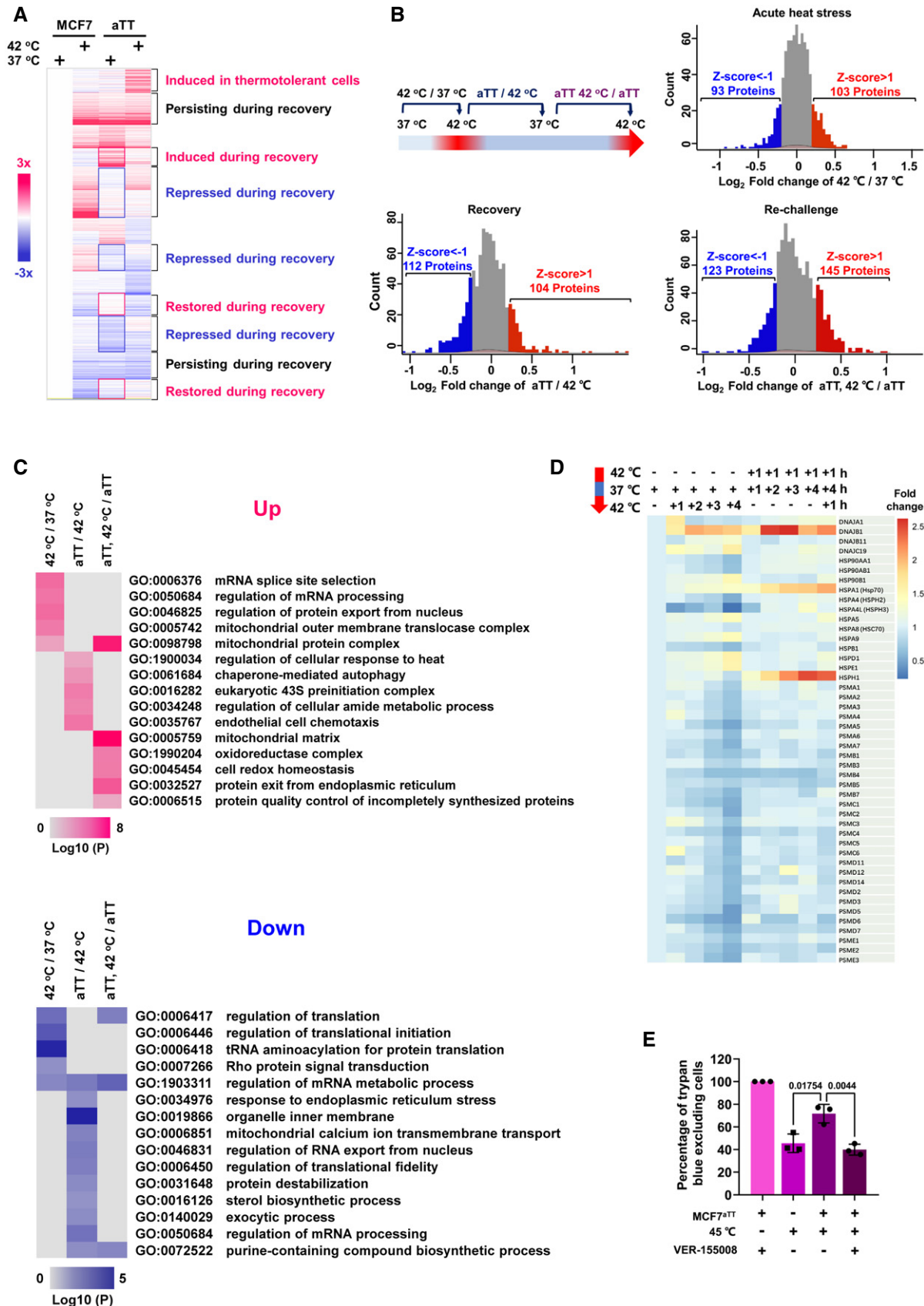


Figure 2.

Figure 2. Proteomic response to heat stress.

- A Heat map summarizing quantitative changes in 1,554 proteins in heat-stressed naïve MCF7 cells and in thermotolerant MCF7^{aTT} cells. The color bar defines the fold changes in protein expression relative to protein levels of MCF7 cells at 37°C.
- B Log₂ fold change distribution of proteins in the indicated comparisons. The fractions of up- and downregulated proteins are highlighted in red and blue. The conditions compared are shown in the scheme on the top left.
- C Heat map showing the enrichment of Gene Ontology functional terms in up- and downregulated proteins shown in (B). *P* values were calculated based on the accumulative hypergeometric distribution (Zhou *et al*, 2019).
- D Heatmap showing changes in the expression of chaperones and proteasome subunits in MCF7 cells during heat shock exposure and recovery (MCF7^{aTT}) as determined by SILAC proteomics.
- E Naïve MCF7 cells and MCF7^{aTT} cells were exposed to the indicated stress conditions for 3 h, and cell viability was assessed by staining dead cells with trypan blue. The bar graphs represent the percentage of trypan blue excluding cells. (means ± SD, *n* = 3, numbers above bars indicate *P* values calculated with the two-stage linear step-up procedure of Benjamini, Krieger, and Yekutieli).

soluble and insoluble fractions by high-speed centrifugation, and fractions were subjected to SDS–PAGE analysis. Staining gels with SYPRO Ruby followed by quantitative imaging revealed no major differences between heat-stressed MCF7 and MCF7^{aTT} cells in the extent of either the soluble or insoluble fractions (Fig 3A). However, exposing MCF7 cells to heat stress in the presence of the HSP70 inhibitor VER-155008 led to a small increase in the insoluble fraction (Fig 3A). This increase was not apparent in MCF7^{aTT} cells (Fig 3A). These data suggested that selective upregulation of the HSPA1-HSPH1-DNAJB1 (HHD) complex discovered in MCF7^{aTT} cells by quantitative proteomics may serve to selectively promote the solubility of a subset of proteins during heat stress.

Maintaining polypeptide solubility is of critical importance for the efficient degradation of polyubiquitylated proteins by the 26S proteasome (Wang *et al*, 2011; Shiber *et al*, 2013; Hjerpe *et al*, 2016). In addition, heat stress is known to trigger polyubiquitylation of damaged proteins and their subsequent clearance by proteasomal degradation (Hjerpe *et al*, 2016). We therefore assessed the solubility of proteins modified with lysine 48 (K48)-linked polyubiquitin chains, which are known to target substrates to the proteasome.

In total MCF7 cell lysate, K48-polyubiquitylated proteins accumulated in response to both heat stress (42°C for 1 h) and the proteasome inhibitor MG132 (Fig 3B). Simultaneous application of heat stress and the HSP70 inhibitor VER-155008 did not lead to a further increase in K48-polyubiquitylated proteins beyond what was observed with heat stress alone. Remarkably, heat-stressed MCF7^{aTT} cells did not display accumulation of K48-polyubiquitylated proteins (Fig 3B). Upon treatment with MG132, heat-induced accumulation of K48-polyubiquitylated proteins was restored, however. This indicates that lack of accumulation of K48-polyubiquitylated proteins in heat-stressed MCF7^{aTT} cells is not due to reduced cellular ubiquitylation activity but to increased proteasomal clearance. Likewise, VER-155008 restored accumulation of K48-polyubiquitylated proteins in heat-stressed MCF7^{aTT} cells, suggesting that the increased levels of HSP70 found in thermotolerant cells serve to promote the degradation of K48-polyubiquitylated proteins.

The majority of polyubiquitin conjugates accumulating upon treatment of naïve MCF7 cells with MG132 were soluble (Fig 3C and D). In contrast, ~ 60% of polyubiquitylated proteins accumulating in response to heat shock were insoluble (Fig 3C and D). Incubation of heat-stressed MCF7 cells with HSP70 inhibitor VER-155008 further increased the fraction of insoluble ubiquitylated proteins to ~ 80%, indicating that HSP70 activity is required to maintain the solubility of heat-damaged polyubiquitylated proteins.

Unlike with MCF7 cells, the majority of polyubiquitin conjugates accumulating in response to heat stress in MCF7^{aTT} cells remained soluble, most likely due to the high amounts of HSPA1 induced in thermotolerant cells (Fig 2D). Indeed, the addition of VER-155008 resulted in an increase in insoluble conjugates, albeit smaller than that observed in naïve MCF7 cells. Thus, unlike proteasome inhibitor, heat stress and HSP70 inhibition caused accumulation of insoluble ubiquitylated proteins that appeared resistant to proteasomal degradation. These data suggest that HSP70 chaperones, and in particular, the HHD complex, which is selectively induced in heat adapted cells, confer thermotolerance, at least in part, by maintaining the solubility and clearance of proteins that were ubiquitylated in response to proteotoxic stress.

Thermotolerant cells are protected from ubiquitylation of newly synthesized proteins through increased recruitment of HSPA1 to polyribosomes

Newly synthesized proteins are known to be preferentially subjected to stress-induced ubiquitylation and proteasomal degradation (Medicherla & Goldberg, 2008; Kim *et al*, 2011; Yau *et al*, 2017). The fraction of nascent proteins undergoing co-translational ubiquitylation in mammalian cells was determined to be 11–14%, numbers that nearly doubled in response to proteotoxic stress or inhibition of HSP70 (Wang *et al*, 2013). The preferential sensitivity of nascent proteins to heat stress-induced ubiquitylation together with the distinct requirement for HSP70 activity in maintaining the solubility of polyubiquitylated proteins raised the intriguing possibility that HSP70-dependent clearance of polyubiquitylated nascent proteins contributes to thermotolerance.

To approach this hypothesis, we first determined the effect of stress on the partitioning of K48-ubiquitylated proteins across a sucrose density gradient which separates translationally active polysomal ribosomes from 40S and 60S monosomes. Although unstressed MCF7 cells showed only a minor portion of K48 polyubiquitylated proteins in polysomal fractions, cells exposed to heat stress or MG132 displayed a strong increase in polysomal ubiquitylation (Fig 4A). The increase in polysomal ubiquitylation contrasted with a reduction in the polysome/monosome ratio, indicating that despite reduced production of nascent proteins in stressed cells, those proteins which were synthesized were extensively decorated with K48 polyubiquitin chains.

Since ribosomes are themselves known to undergo ubiquitylation in response to stress conditions (Higgins *et al*, 2015; Sugiyama *et al*, 2019), we sought to rule out that the K48 polyubiquitin signals

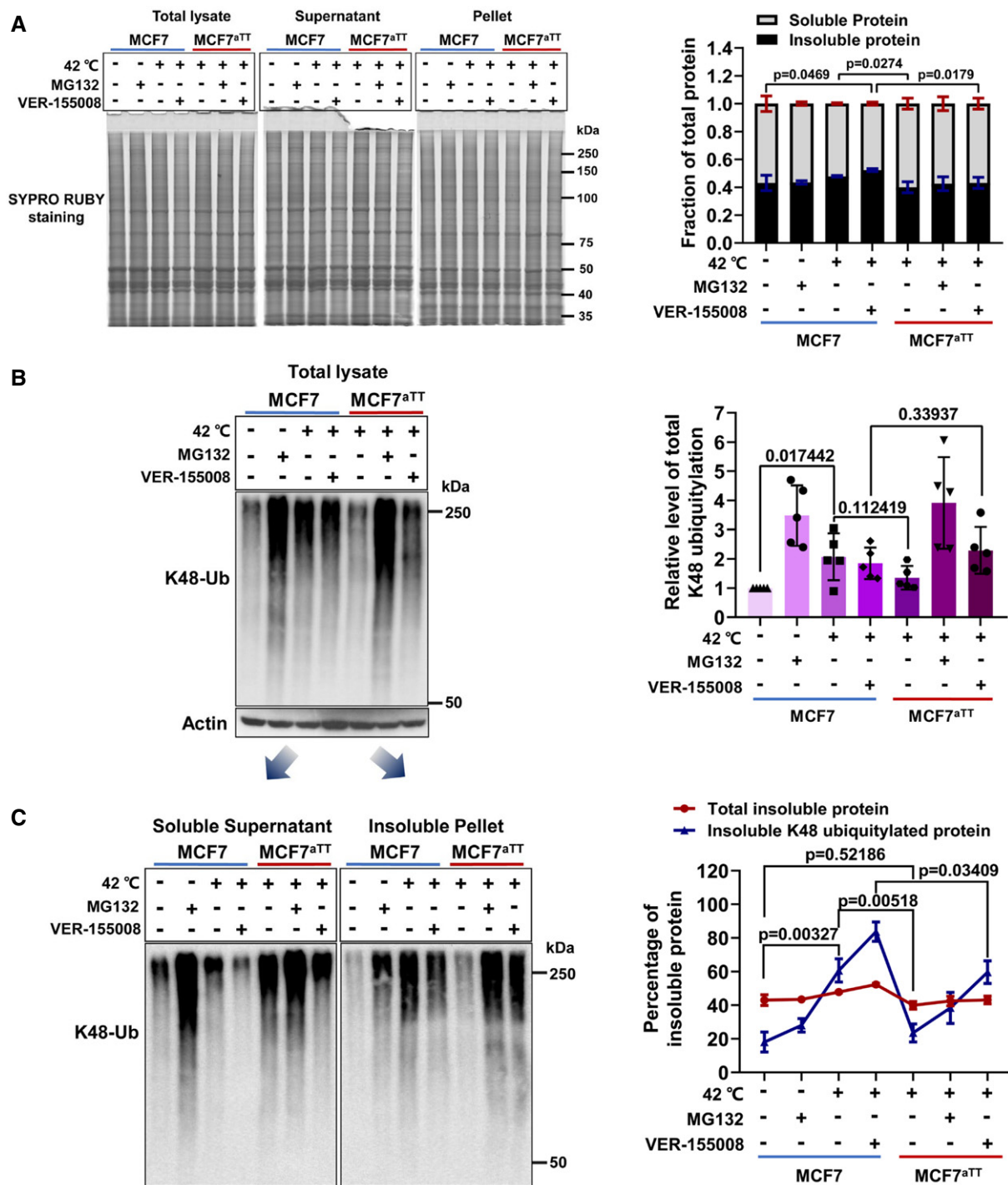


Figure 3. Effect of HSP70 activity on the solubility of polyubiquitylated proteins.

A Whole lysates of MCF7 and MCF7^{aTT} cells exposed to heat shock and/or proteasome (MG132, 20 μM, 1 h) and HSP70 (VER-155008, 50 μM, 1 h) inhibitors were prepared as described in Materials and Methods. Total lysate, soluble fractions, and insoluble fractions were stained by SYPRO Ruby (left) and quantified (right). (means ± SD, n = 3, numbers above the bars indicate P values calculated with the two-stage linear step-up procedure of Benjamini, Krieger, and Yekutieli).

B The same total lysates as shown in (A) were assayed for the level of K48-linked polyubiquitin. Actin is shown as a reference. The levels of K48-linked polyubiquitin were quantified from multiple independent repeats. (means ± SD, n = 5, numbers above the bars indicate P values calculated with the two-stage linear step-up procedure of Benjamini, Krieger, and Yekutieli).

C The soluble and insoluble fractions shown in (A) were assayed for the level of K48-linked polyubiquitin, and polyubiquitylated proteins were quantified (blue line graph, means ± SEM, n = 4, numbers above the bars indicate P values). The data for bulk protein obtained in (A) were overlaid onto the graph for comparison (red line, means ± SEM, n = 3).

Source data are available online for this figure.

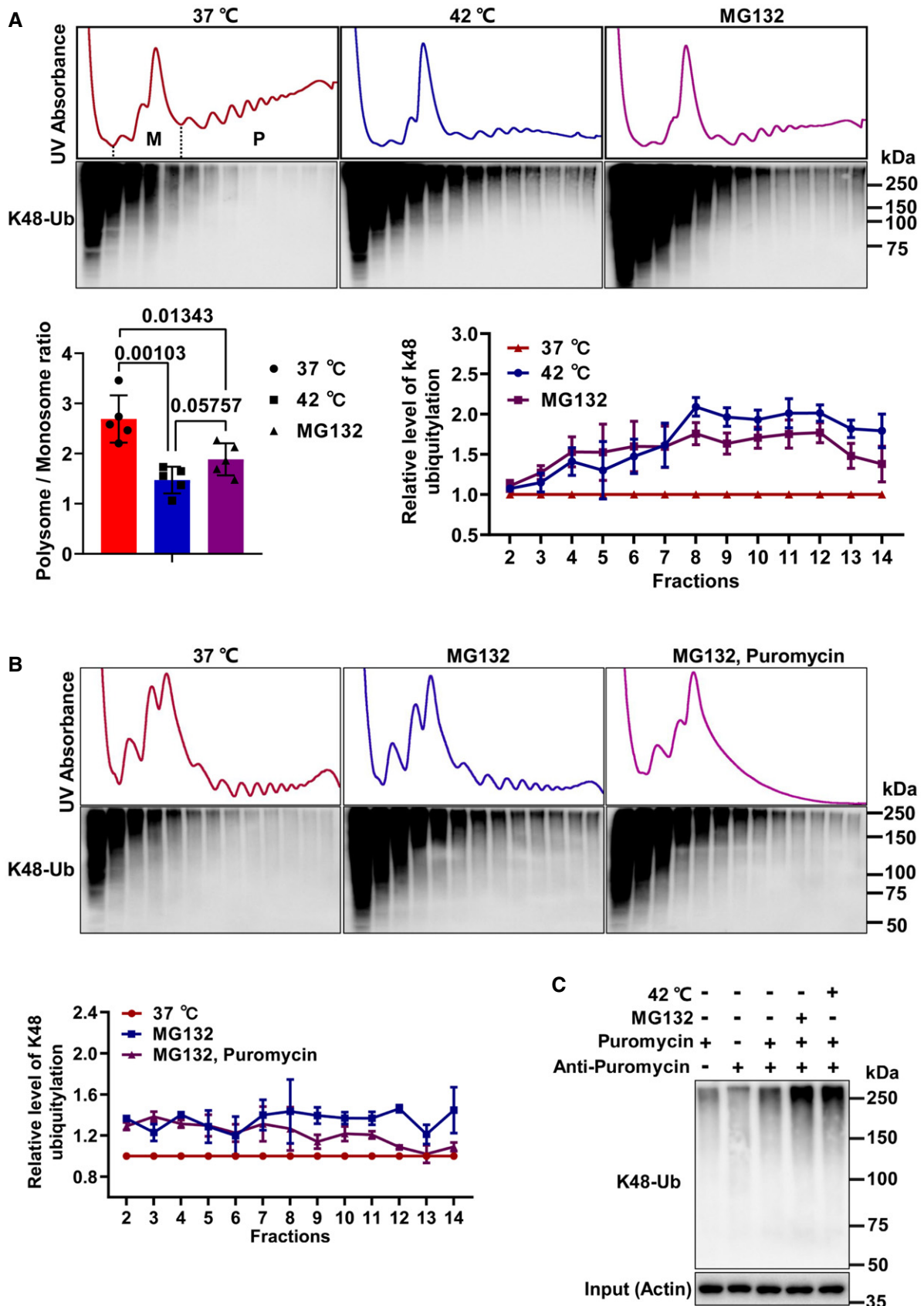


Figure 4.

Figure 4. Ubiquitylation of nascent/newly synthesized proteins during acute heat stress or exposure to the proteasome inhibitor MG132.

- A Lysates from MCF7 cells exposed to the proteasome inhibitor MG132 (20 μ M, 1 h) or to heat shock (42°C, 1 h) were subjected to sucrose density gradient centrifugation. Monosomal and polysomal fractions were quantified from the UV traces at 254 nm. Monosomes eluting in fractions 4–6 and polysomes in fractions 7–14 were quantified and polysome to monosome (P/M) ratios were calculated. Average ratios and the individual datapoints ($n = 5$) are displayed in a bar graph (means \pm SD). Numbers above the bars represent P values calculated with the two-stage linear step-up procedure of Benjamini, Krieger, and Yekutieli. Gradient fractions were assayed for the presence of lysine (K) 48-linked polyubiquitylated proteins by immunoblotting with K48 linkage-specific antibodies. The line graph on the right is a quantification of K48-linked polyubiquitin across the gradients relative to the levels obtained in MCF7 cells maintained at 37°C (means \pm SEM, $n = 4$).
- B The same experiment as described in (A) but with MCF7 cells exposed to MG132 (20 μ M, 1 h) or puromycin (100 μ g/ml, 10 min). Means \pm SEM, $n = 2$.
- C Lysate from MCF7 cells exposed to MG132 (20 μ M, 1 h) or puromycin (100 μ g/ml, 10 min) as indicated was subjected to immunoprecipitation with anti-puromycin antibodies, followed by assaying for co-precipitation of K48-ubiquitylated proteins. Actin is shown as a reference.

Source data are available online for this figure.

observed across the sucrose density gradient merely reflected ubiquitylation of ribosomal proteins (RPs). By immunoblotting, we did not observe species of RPS19 or RPL7 that would be consistent with either mono- or polyubiquitylated forms (Appendix Fig S1). These findings are in agreement with previous reports that RP ubiquitylation occurs primarily through monoubiquitin and is selectively triggered by ER stress but not by heat stress or inhibition of HSP70 (Higgins *et al*, 2015; Nguyen *et al*, 2017). Likewise, RP polyubiquitylation in yeast was shown to occur with K63-linked chains (Sugiyama *et al*, 2019) rather than the K48-linked chains we observed.

To further establish that stress-induced polysomal K48 polyubiquitylation reflects modification of nascent proteins, we tested whether releasing nascent chains from polysomes by incubating cells with the tRNA analog puromycin would diminish polysomal levels of K48 polyubiquitylated proteins. Indeed, release of nascent chains decreased the K48 polyubiquitin signal in heavy polysomes (Fig 4B, Appendix Fig S2), suggesting that the bulk of this signal was derived from nascent polypeptides. Residual polysomal K48-polyubiquitin signal in the puromycin sample may be due to less than complete release of nascent chains. In a separate experiment, immunopurification of nascent puromycylated proteins from MCF7 cells showed co-purification of K48 polyubiquitin chains in a manner that was substantially increased by heat stress and MG132 (Fig 4C). Thus, in agreement with previous studies (Wang *et al*, 2013; Yau *et al*, 2017), nascent protein polyubiquitylation is stress-inducible and readily apparent in polyribosomes.

Remarkably, thermotolerant MCF7^{aTT} cells did not show significant accumulation of K48 polyubiquitin in polysomal fractions upon heat stress (Fig 5A). However, treatment with VER-155008 restored polysomal polyubiquitin despite severe suppression of the polysome/monosome ratio (Fig 5B). This finding suggests that the induction of HSP70 activity in MCF7^{aTT} cells we found by proteomics is essential for preventing both polysomal accumulation of polyubiquitylated—and hence presumably damaged—nascent proteins and translational arrest upon heat stress. In support of this conjecture, we observed that induction of HSPA1 in MCF7^{aTT} cells resulted in its increased co-fractionation with polysomes (Fig 5C), a finding that is consistent with the well-established interaction of HSPA1 with ribosomes (Jaiswal *et al*, 2011).

As in naïve MCF7 cells, MG132 led to pronounced accumulation of polysomal K48 polyubiquitin in heat-challenged MCF7^{aTT} cells (Fig 5B). Once again, this illustrates that lack of accumulation of polyubiquitylated species in the absence of MG132 is due to the HSP70-dependent increase in the ability of MCF7^{aTT} cells to rapidly clear damaged proteins via the proteasome rather than to preventing

protein damage or inhibiting the ubiquitylation machinery of thermotolerant cells.

To test whether, as observed with total cellular protein (Fig 3), HSP70 activity also maintained the solubility of ubiquitylated proteins present in polysomal fractions, we sedimented polysomes from MCF7 and MCF7^{aTT} cells exposed to heat stress with or without VER-155008 through a 30% sucrose cushion, followed by dissociation of 80S ribosomes with EDTA. EDTA-mediated disassociation of polysomes into 40S and 60S was verified by sucrose density gradient centrifugation (Appendix Fig S3). Resulting protein lysates were separated into soluble supernatant and insoluble pellet fractions by high-speed centrifugation, and fractions were subjected to immunoblotting with K48-ub antibodies. Heat stress led to stronger accumulation of polysome-derived K48-ub proteins in the insoluble fraction isolated from MCF7 cells than from heat-resistant MCF7^{aTT} cells (Fig 5D). VER-155008 restored accumulation of insoluble polysome-derived proteins modified with K48 polyubiquitin in both MCF7 and MCF7^{aTT} cells, indicating that HSP70 is limiting for maintaining the solubility of K48-ubiquitylated proteins co-fractionating with polysomes, which most likely represent nascent polypeptides.

HSP70 promotes proteasome recruitment to polysomes

The above studies suggested a profound role of HSP70 activity in targeting polyubiquitylated nascent polypeptides for proteasomal degradation, a process that would be more efficient in thermotolerant cells with increased levels of the HHD complex. This would necessitate a mechanism for recruiting the proteasome to elongating 80S ribosomes. Notably, the 26S proteasome and HSP70 are known to physically interact with ribosomes (Guerrero *et al*, 2008; Sha *et al*, 2009; Wang *et al*, 2015a; Wang *et al*, 2015b), raising the possibility that HSP70 may promote proteasome recruitment to ribosomes.

Measuring proteasome activity in sucrose density gradient fractions, we observed a small fraction of total cellular proteasome activity co-fractionating with polysomes of MCF7 cells (Fig EV2A). The co-fractionation depended on the integrity of polysomes as it was abolished by incubating the cell lysate with RNase I (Fig EV2A), thus suggesting that it reflected interaction of proteasomes with active ribosomes. Using the same assay, we found increased accumulation of proteasomes in polysomal fractions upon heat stress or upon incubation of cells with MG132 (Fig 6A). This was also apparent by immunoblotting with proteasome antibodies in MCF7 cells as well as another cell line, AD293 (Fig EV2B).

Since proteasome accumulation correlated with levels of polysomal K48 polyubiquitin (compare Figs 4A and 6A), we asked

whether it depended on enhanced ubiquitylation of nascent peptides. To test this, we added recombinant deubiquitylating enzyme USP2 to cell lysate prior to sucrose density gradient separation. Despite extensive removal of K48-linked polyubiquitin from polysomal fractions by USP2 (Fig EV3A–C), proteasome recruitment was only minimally affected (Fig EV3D). These findings suggest that proteasome recruitment to polysomes in response to proteotoxic stress occurs independently of nascent chain ubiquitylation.

Since neither proteasome abundance nor activity and assembly into 26S particles was altered by heat stress (Appendix Fig S4), we

tested whether polysomal accumulation of proteasome activity in heat-stressed cells was due to increased recruitment of the proteasome to polyribosomes. Lysate of MCF7 cells exposed to heat stress or MG132 was spun through a 30% sucrose cushion to isolate polysomes, followed by immunoblotting for co-fractionating proteasome subunits. Exposure to heat stress or MG132 led to a strong increase in 19S and 20S proteasome subunits retrieved in polysomal fractions (Fig 6B).

To determine whether this co-fractionation reflected physical ribosome-proteasome interactions, we collected polysomal fractions

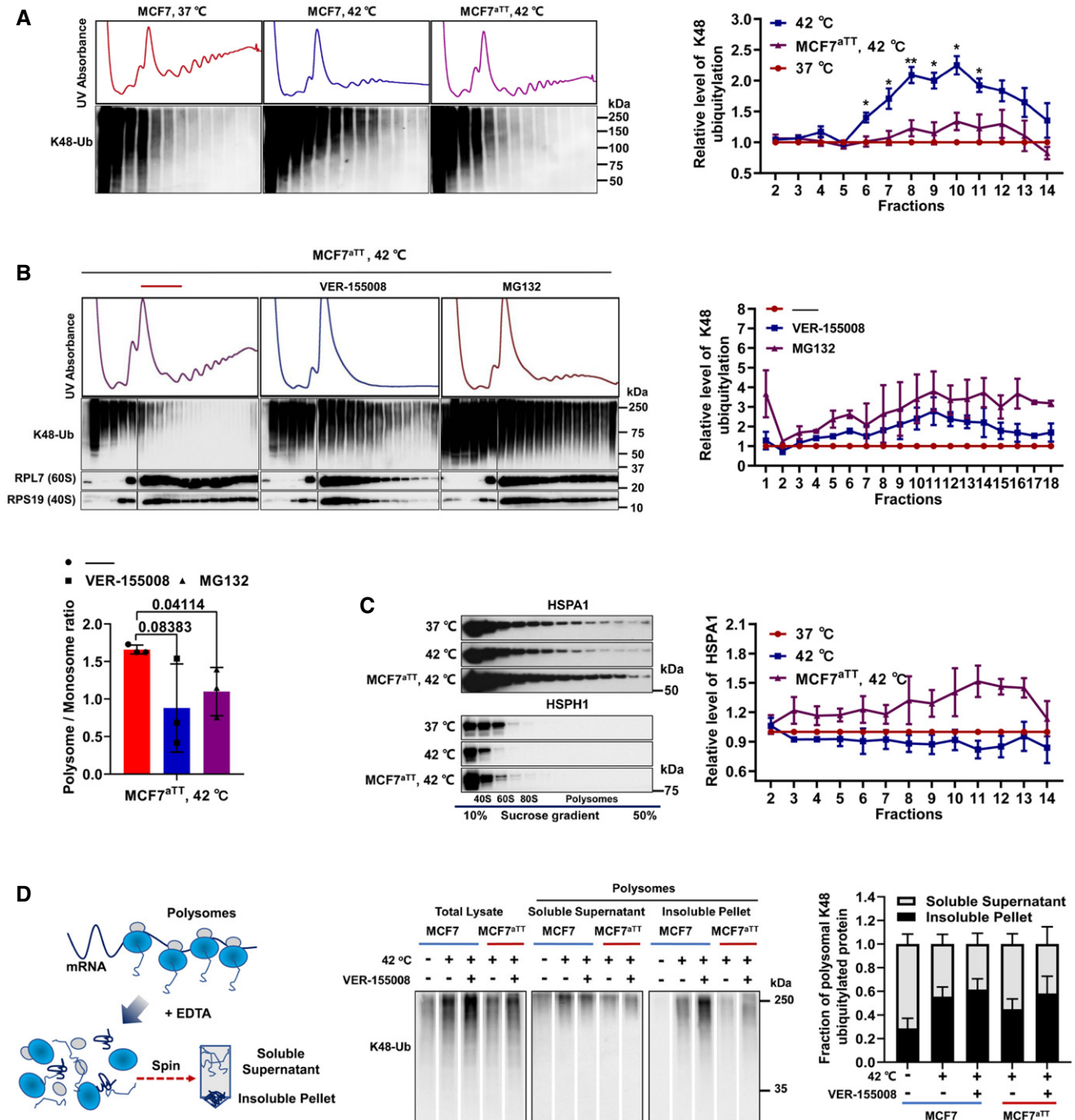


Figure 5. Thermotolerance depends on both proteasome and HSP70 activities.

- A Similar experiment as described in (Fig 4A) with naïve MCF7 and thermotolerant MCF7^{aTT} cells as indicated. Means \pm SEM, $n = 3$, * $P < 0.05$, ** $P < 0.01$ (calculated with the two-stage linear step-up procedure of Benjamini, Krieger, and Yekutieli).
- B Same experiment as in (A) with thermotolerant MCF7^{aTT} cells incubated with the HSP70 inhibitor VER-155008 (50 μ M, 1 h) or MG132 (20 μ M, 1 h). The signal obtained for ribosomal protein RPS19 and RPL7 is shown for reference, documenting residual polysomes despite the flat UV trace. Right panels are quantifications of K48-ub (means \pm SEM, $n = 2$), black vertical lines indicate splicing of lanes that were run on different gels due to limitations in lane capacity. The bar graphs represent the P/M ratios (means \pm SD, $n = 3$, numbers above bars indicate P values calculated with the two-stage linear step-up procedure of Benjamini, Krieger, and Yekutieli).
- C Sucrose density gradient fractions described in (B) were assayed for partitioning of HSPA1 and HSPH1 by immunoblotting. HSPA1 data were quantified in a line graph (means \pm SEM, $n = 4$).
- D Cell lysate was spun through a 30% sucrose cushion to pellet polysomes. Nascent proteins were released from polysomes by dissociating 80S ribosomes with EDTA (see Appendix Fig S3). Soluble and insoluble fractions were prepared by centrifugation and assayed for the level of K48-linked polyubiquitin. The levels of K48-linked polyubiquitin were quantified (means \pm SD, $n = 3$). Immunoblots within black squares were run on the same gel but irrelevant lanes were removed as indicated by white lines.

Source data are available online for this figure.

from a sucrose density gradient, subjected them to immunoprecipitation with anti-RPS19 antibodies, and analyzed the immunopurified material by LC-MS/MS. Label-free quantification revealed ready co-purification of 80S ribosomes with proteasome subunits (Fig 6C). The interaction was increased when cells were exposed to MG132. In addition, MG132 led to an apparent stabilization of the interaction between 19S and 20S proteasomes (Fig 6C). In a similar experiment, we digested polysomal fractions with RNase I to release 80S particles. We then used antibodies against RPL7 to immunopurify 80S complexes and determined co-purification of proteasome subunits by immunoblotting. We found that several 19S and 20S proteasome subunits co-purified with polysomal ribosomes (Fig EV4A). For ADRM1 and PSMA1–6, we observed an apparent increase in ribosome interaction in response to heat stress and MG132, especially when accounting for the lower retrieval of polysome-derived 80S complexes from the stressed cells (Fig EV4A). In a reciprocal experiment with total cell lysate, we found that two different methods of purifying 26S proteasomes led to readily detectable and specific co-purification of 40S and 60S RPs (Fig EV4B and C).

To biochemically confirm that HSP70 activity promotes the recruitment of the 26S proteasome to nascent peptides, we used puromycin labeling and pull-down to isolate nascent peptides from MCF7^{aTT} cells with increased levels of HSPA1 and other HHD subunits. Some cell samples also received VER-155008 to inactivate HSP70 or MG132 to inhibit proteasome activity. Binding of proteasome subunits ADRM1 and PSMA1–6 to nascent chains observed in cells treated with MG132 was completely dependent on HSP70 activity, since it was abolished by VER-155008 (Fig 6D).

In the above experiment with heat-stressed MCF7^{aTT} cells, we noticed that the HSP70-dependent interaction of the proteasome with nascent chains was only apparent when cells were treated with MG132. This finding was unexpected considering our observation that proteasome recruitment to polysomes was readily apparent in heat-stressed MCF7 cells in the absence of MG132 (Fig 6A). We therefore explored the possibility that increased recruitment of HSPA1 to polysomes in thermotolerant MCF7^{aTT} cells might promote proteasomal degradation of ubiquitylated nascent proteins thus reducing the dwell time of the proteasome on ribosomes. Indeed, when proteasomal degradation was inhibited by MG132, the proteasome appeared trapped in the polysomal fraction of MCF7^{aTT} cells as indicated by proteasome activity assay and immunoblotting for the 20S subunit PSMB1 (Fig 6E). This apparent trapping

depended on HSPA1 activity as it was reduced by VER-155008 (Fig 6E). The dependence of proteasome recruitment to polysomes on HSPA1 activity was also readily apparent in naïve MCF7 cells exposed to heat shock (Fig EV5). Taken together, these findings firmly suggest that HSP70 serves to recruit the proteasome to heat-damaged nascent proteins thus promoting quality control of newly synthesized proteins and thermotolerance.

Inactivation of HSPH1 curbs thermotolerance of esophageal cancer cells

To test the above conjecture, we sought to genetically inactivate the HHD complex. We were unsuccessful in disrupting HSPA1 or HSPH1 by CRISPR/Cas9 in MCF7 cells, possibly due to the near tetraploid genome of these cells. A search of the Cancer Cell Line Encyclopedia revealed esophageal cancer cell lines as the highest expressors of *HSPH1* mRNA among groups of human cancer cell lines derived from 40 different tissues (Appendix Fig S5A). Likewise, esophageal cancer cell lines ranked seventh for expression of *HSPA1* mRNA (Appendix Fig S5B). We therefore attempted to use CRISPR/Cas9 to knock out *HSPA1* and *HSPH1* in the human esophageal cancer cell line KYSE150. Although we were unsuccessful in disrupting *HSPA1* possibly indicating essentiality, we obtained several viable *HSPH1* knockout cell lines (KYSE150^{HSPH1-/-}; Fig 7A).

KYSE150^{HSPH1-/-} cells were only slightly more sensitive to heat shock at 45°C than the parental KYSE150 cells, which were relatively heat-resistant compared to MCF7 cells (Fig 7B, compare Fig 1B). However, upon additional challenge with MG132 and VER-155008, *HSPH1* knockout cells showed marked thermosensitivity (Fig 7C). KYSE150^{HSPH1-/-} cells were also deficient in developing adaptive thermotolerance. Although parental KYSE150 cells rendered thermoresistant through the same temperature shifting scheme used for MCF7^{aTT} cells (Fig 1A) no longer showed polysomal enrichment of polyubiquitylated proteins after heat shock for 1 h, KYSE150^{HSPH1-/-} cells subjected to the same treatment still accumulated large amounts of polyubiquitylated proteins in polysomes (Fig 7D). As with VER-155008-treated MCF7 cells (Fig 3C), *HSPH1*-deficient KYSE150 cells were also defective in maintaining the solubility of K48 ubiquitylated proteins accumulating upon heat shock (Fig 7E) thus providing further genetic support for the conception that the HHD complex mediates thermotolerance by

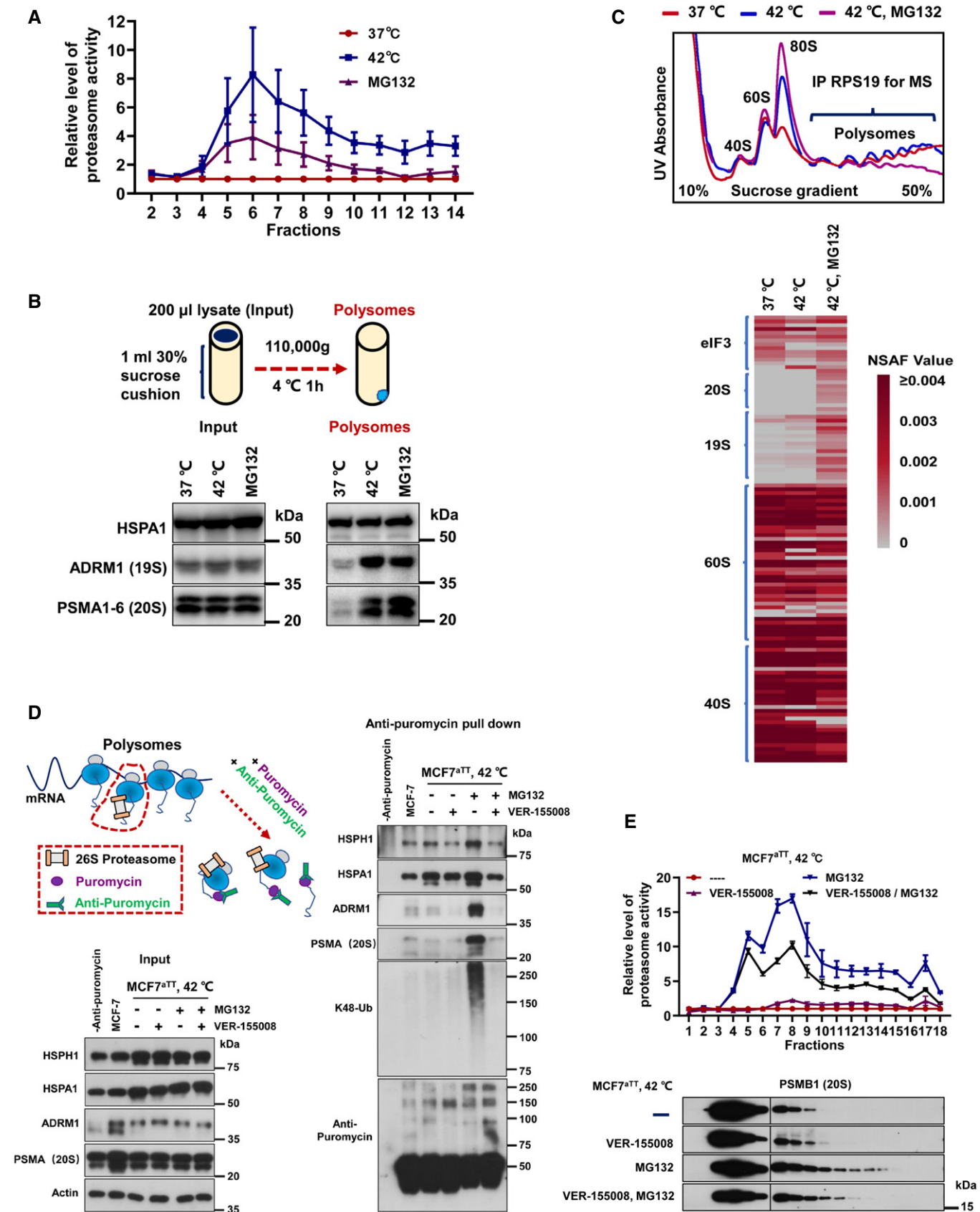


Figure 6. HSP70 promotes proteasome recruitment to polysomes.

- A Trypsin-like proteasome activity determined in sucrose density gradient fractions as described in Fig 4A using an in vitro assay. Results are shown relative to the proteasome activity obtained in MCF7 cells maintained at 37°C (means \pm SEM, $n = 4$).
- B MCF7 cells were exposed to the proteasome inhibitor MG132 (20 μ M) or 42°C for 1 h after which an equal amount of cell lysate was spun through a 30% sucrose cushion. Resulting polysomes were assayed for the levels of 26S proteasome subunits and HSPA1.
- C Cell lysates from MCF7 cells maintained under the conditions indicated were fractionated by sucrose density gradient centrifugation. Polysomal fractions were subjected to immunoprecipitation with RPS19 antibody, and precipitates were analyzed by quantitative LC-MS/MS. The heat map represents normalized spectral abundance factors (NSAF).
- D Total cell lysates were prepared from naïve MCF7 and thermoresistant MCF7^{TRT} cells, and puromycin labeled peptides were pulled down as illustrated in the scheme. Precipitates were assayed for the presence of K48-linked polyubiquitin, chaperones, and proteasome subunits by immunoblotting.
- E Partitioning of the 20S proteasome subunit PSMB1 along the sucrose gradient under the indicated conditions was assessed by immunoblotting, black vertical lines indicate splicing of lanes that were run on different gels due to limitations in lane capacity. The line graph on the top shows trypsin-like proteasome activity in the same fractions (means \pm SD, $n = 3$).

Source data are available online for this figure.

solubilizing ubiquitylated proteins in order to enable their clearance by the proteasome.

Remarkably, however, heat-induced recruitment of the proteasome to polysomes did not depend on HSPH1 as it occurred in both parental KYSE150 and KYSE150^{HSPH1-/-} cells (Fig 7F). This finding indicates that polysomal recruitment of the proteasome uniquely requires HSPA1 but not HSPH1. We also observed that KYSE150^{TRT} cells that were rendered thermoresistant and then challenged with heat shock displayed a lower level of proteasome recruitment to polysomes than naïve KYSE150 cells (Fig 7F). This reiterates the observation we previously made in MCF7^{TRT} cells, which we attributed to a reduced polysomal dwell time of the proteasome in thermoresistant cells based on MG132-induced trapping of the proteasome in polysomal fractions (Figs 6E and EV5). Proteasome recruitment to polysomes was also reduced in KYSE150^{HSPH1-/-} cells undergoing the thermotolerance-inducing scheme followed by heat shock (Fig 7F) even though they accumulated large amounts of K48 ubiquitin in polysomes (Fig 7D) which is most likely in an insoluble, proteasome-resistant state (Fig 7E). This observation is consistent with our finding that proteasome recruitment to nascent proteins is largely independent of ubiquitylation (Fig EV3) and suggests an unknown mechanism by which the proteasome disengages from ribosomes when it encounters degradation-resistant ubiquitin conjugates.

HSPH1 expression is increased in digestive tract cancers and is required for tumor formation in mice

To put our in vitro observations into a physiological context, we turned to esophageal squamous cell carcinoma (ESCC), the fourth most common cancer in China. We performed immunohistochemistry on paraffin-embedded tissue samples of a set of ESCCs and oral squamous carcinoma (OSCCs) and matching normal tissues. Quantitative scoring revealed strong overexpression of cytoplasmic and nuclear HSPH1 in ESCCs and OSCCs compared to the surrounding normal tissue (Fig 8A ad B). Although no difference was observed between tumors and controls for the expression of HSPA1 in these sets of samples, high *HSPH1* mRNA in a series of 182 ESCCs strongly correlated with poor prognosis ($P = 0.035$; Fig 8C). Similar correlations with unfavorable prognoses exist for large panels of head and neck as well as liver cancers (Appendix Fig S6). These data suggest that cancers obtain a growth and survival advantage by upregulating the co-translational thermotolerance pathway.

To test this conjecture, we measured the ability of parental KYSE150 and KYSE150^{HSPH1-/-} cells to form tumors in nude mice. Cells were injected subcutaneously, and tumor sizes were measured over a period of 29 days. Tumors derived from KYSE150^{HSPH1-/-} cells were impaired in growth as shown by measurement of average tumor sizes over time, mean terminal tumor weights, and individual tumor sizes (Fig 8D and E). Immunohistochemistry and immunoblotting confirmed severe depletion of HSPH1 protein in KYSE150^{HSPH1-/-} tumors (Appendix Fig S7). We also ascertained that the differences in tumor sizes were not reflected in different body weights of host animals (Appendix Fig S8).

Discussion

HSPA1/HHD and quality control of nascent/newly synthesized proteins

Employing proteomic profiling during acute heat stress and recovery, we found response patterns consistent with promotion of cellular integrity and survival. The most striking change was a robust upregulation—uniquely in thermotolerant cells—of HSPA1 and its co-factors HSPH1 and DNAJB1 which are known to form the HHD chaperone complex. HHD has emerged as an intensely studied protein disaggregation/refolding machine (Mogk *et al*, 2018). Although its biochemical mechanisms are becoming increasingly well understood (Shorter, 2011; Nillegoda *et al*, 2015; Faust *et al*, 2020; Wentink *et al*, 2020), its physiological roles in stress defense and human disease remain largely obscure. Several of our findings suggest that HSPA1, alone and within HHD, plays hitherto unexplored roles in the quality control of nascent/newly synthesized proteins that become especially apparent during recovery from heat stress:

- i Among seventeen HSPs quantitatively profiled, including six HSP70 family members and three HSP70 NEFs, only HSPA1, HSPH1, and DNAJB1 were selectively upregulated during acquisition of thermotolerance, making them the most abundant members of their respective chaperone families in heat adapted cells (Figs 2D and EV1C).
- ii Upregulation of HSP70 activity in thermotolerant cells—and thus most likely HSPA1 as part of HHD—does not appear to be required for maintaining bulk protein solubility in response to heat stress. Rather, HHD, as shown by VER-155008 treatment

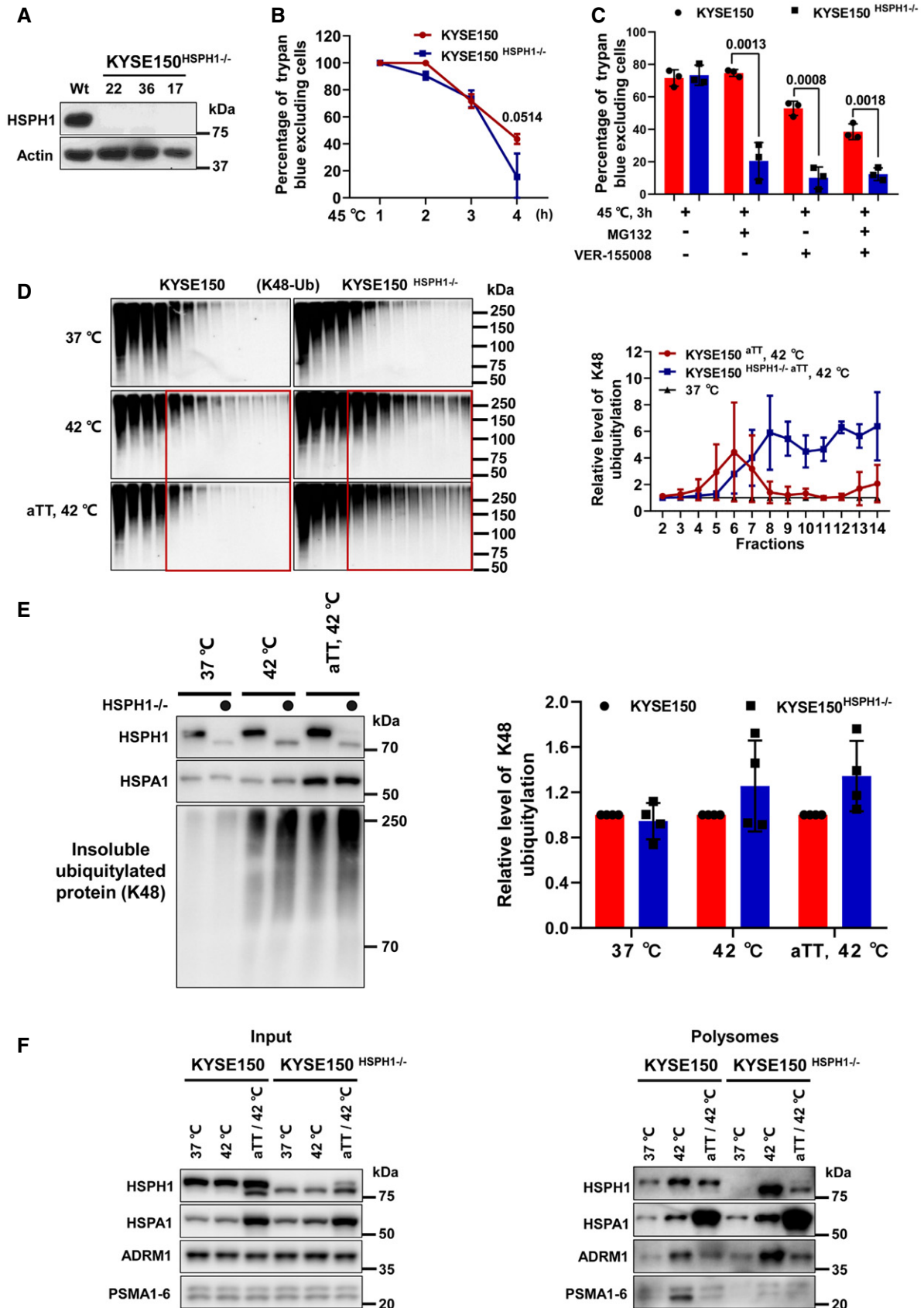


Figure 7.

Figure 7. Effect of HSPH1 depletion on co-translational quality control in esophageal cancer cells.

- A Immunoblot of individual clones of KYSE150 cells in which HSPH1 was disrupted by CRISPR/Cas9 targeting (KYSE150^{HSPH1-/-} cells).
- B Effect of disrupting HSPH1 on stress sensitivity. KYSE150 and KYSE150^{HSPH1-/-} cells were exposed to heat stress (45°C; means ± SD, *n* = 3), and cell viability was assessed by staining dead cells with trypan blue.
- C KYSE150 and KYSE150^{HSPH1-/-} cells were exposed to the indicated stress conditions and cell viability was assessed by staining dead cells with trypan blue. Graphs represent means ± SD, *n* = 3, numbers above bars indicate *P* values calculated with the two-stage linear step-up procedure of Benjamini, Krieger, and Yekutieli.
- D KYSE150 and KYSE150^{HSPH1-/-} cells, either naïve or subjected to the aTT temperature shifting scheme, were exposed to the indicated temperature and cell lysates were separated by sucrose density gradient centrifugation. K48-linked polyubiquitin was detected by immunoblotting of gradient fractions (left panel). Signals were quantified and displayed as a line graph (right panel, means ± SEM, *n* = 2). The red boxes highlight the pronounced differences in polysomal polyubiquitylation between KYSE150 and KYSE150^{HSPH1-/-} cells.
- E Whole lysates of KYSE150 and KYSE150^{HSPH1-/-} cells exposed to the indicated temperature conditions (aTT scheme and heat shock) were fractionated into soluble and insoluble fractions as described in Materials and Methods. Insoluble fractions were assayed for the level of K48-linked polyubiquitin (left panel). Total levels of HSPA1 and HSPH1 are shown for reference. K48 ubiquitin signals were quantified and displayed in a bar graph (means ± SD, *n* = 4).
- F Lysates of KYSE150 and KYSE150^{HSPH1-/-} cells exposed to the indicated temperature conditions (aTT scheme and heat shock) were obtained, and polysomes were isolated by centrifugation through a 30% sucrose cushion. Whole cell lysates (left panel) and the polysomal pellets (right panel) were assayed by immunoblotting for the levels of HSPH1, HSPA1, and proteasome subunits.

Source data are available online for this figure.

and knockout of HSPH1, maintains the solubility of polysomal proteins modified with K48-polyubiquitin in response to heat stress (Figs 3C and 5D). This is consistent with the previous demonstration that HSPH1 participates in the solubilization of heat-induced polyubiquitylated protein aggregates required for their proteasomal clearance (Hjerpe *et al.*, 2016).

- iii Our data show that HSP70 activity is required for efficient recruitment of 26S proteasomes to polysomes in response to acute heat stress and probably also during thermotolerance. We attribute this function mainly to HSPA1 because it was the most abundant HSP70 protein in thermotolerant cells and thus likely the main target of the chemical HSP70 inhibitor VER-155008 (Fig EV1B). Other HSP70 proteins induced during heat stress, HSPA5 (GRP78, BiP) and HSPA9 (GRP75), are localized in the endoplasmic reticulum and in mitochondria and thus unlikely to mediate quality control of nascent/newly synthesized proteins as studied here.

The exact molecular function of HSPA1 in proteasome recruitment to ribosomes remains unknown. As it occurs equally in response to acute heat stress of naïve MCF7 cells where HSPH1 has not yet been induced (Fig 2D) and in KYSE150^{HSPH1-/-} cells (Fig 7F), proteasome recruitment to ribosomes appears independent of HSPH1. One possibility is that HSPA1, through distinct binding sites on the ribosome and the proteasome, bridges their interaction within a particle we dubbed the “translasome” (Sha *et al.*, 2009). As

such, increased HSPA1 in heat-stressed cells may trigger de novo ribosome-proteasome complexes independently of nascent chain ubiquitylation (Fig EV3) and potentially unaided by nascent chains entirely. Alternatively, increased interaction of HSPA1 with nascent chains may promote proteasome recruitment. Here, HSPA1 might function in the sense of a proteasome shuttle (Shiber & Ravid, 2014), albeit in a ubiquitylation-independent manner (Fig EV3). Hybrid forms of these models are thinkable where nascent chains would stabilize HSPA1-ribosome and HSPA1-proteasome interactions thus promoting ribosome-proteasome interactions.

Implications for heat stress response

Our studies of the adaptive thermotolerance paradigm also revealed surprising insights that spur a refined model of the molecular events orchestrating the cellular response to heat stress (Fig 9). For one, we observed that K48-linked polyubiquitin chains accumulate strongly in polysomes of acutely stressed cells despite HSPA1-enhanced proteasome recruitment to ribosomes. This suggests that during the acute stress response, proteasomal degradation of nascent/newly synthesized proteins is halted. Mechanistically, this might, for example, involve inhibition of proteasomal degradation by autoubiquitylation of proteasome subunit ARDM1/RPN13 (Besche *et al.*, 2014). Given our demonstration that HSPH1 is required for the solubilization of polyubiquitylated proteins, it is also likely that HSPH1 is limiting for efficient degradation during the acute stress

Figure 8. Expression of HSPA1 and HSPH1 in human carcinomas.

- A Representative micrographs of tissue sections derived from oral squamous cell carcinomas (OSCC) and esophageal squamous cell carcinomas (ESCC) stained with the indicated antibodies by immunohistochemistry (IHC). Top panels show routine H&E staining. Black squares point to regions magnified in the adjacent panels to the right.
- B IHC staining of HSPA1 and HSPH1 was performed for the indicated numbers of normal, OSCC, and ESCC tissues. Staining intensity was scored as described in Materials and Methods.
- C Kaplan–Meier plots showing the correlation between HSPH1 mRNA expression level and the survival of patients with ESCC. The expression data were obtained from and visualized with KM Plotter (www.kmplot.com, Nagy *et al.*, 2018) using the Pan Cancer algorithm at default settings.
- D KYSE150 and KYSE150^{HSPH1-/-} cells were injected into nude mice, and xenograft tumor growth was monitored over time (left panel; mean tumor volume ± SEM, *n* = 4 with five animals per *n*). Mean tumor weights at the end of the experiments were determined (means ± SD, *n* = 4 with 5 animals per *n*, number above the bar graph represent *P* values, **P* < 0.05, ***P* < 0.01 [calculated with the two-stage linear step-up procedure of Benjamini, Krieger, and Yekutieli]).
- E Macroscopic images of representative tumors derived from KYSE150 and KYSE150^{HSPH1-/-} cells (shown are tumors from two of the four independent experiments).

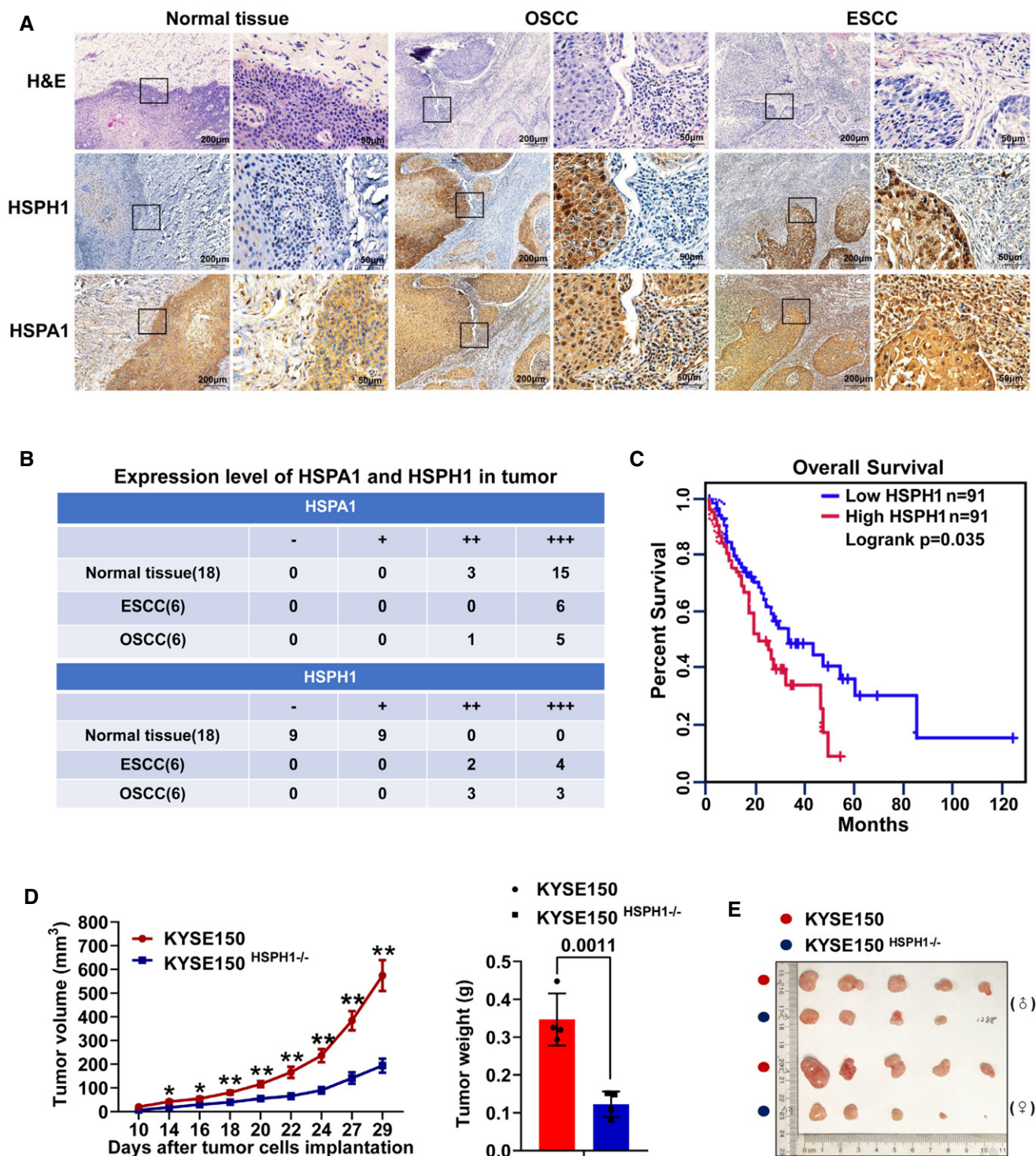


Figure 8.

response where its expression has not yet been induced. A transient period of inhibition of proteasomal degradation following acute stress may afford chaperones the time needed to refold heat-damaged proteins (Wallace *et al*, 2015; Määttä *et al*, 2020). HSPA1-assisted proteasome recruitment to ribosomes may thus poise cells for rapid clearance of those proteins that are irreversibly heat-

damaged, pending a recovery signal. This signal may be given by the boost in the HHD complex after relief from acute heat stress, resulting in the activation of proteasomal degradation and resumption of protein synthesis. In the absence of this relief signal, cells may remain locked in translational shutdown and ultimately succumb to irreparable damage as seen in HSPH1 knockout cells

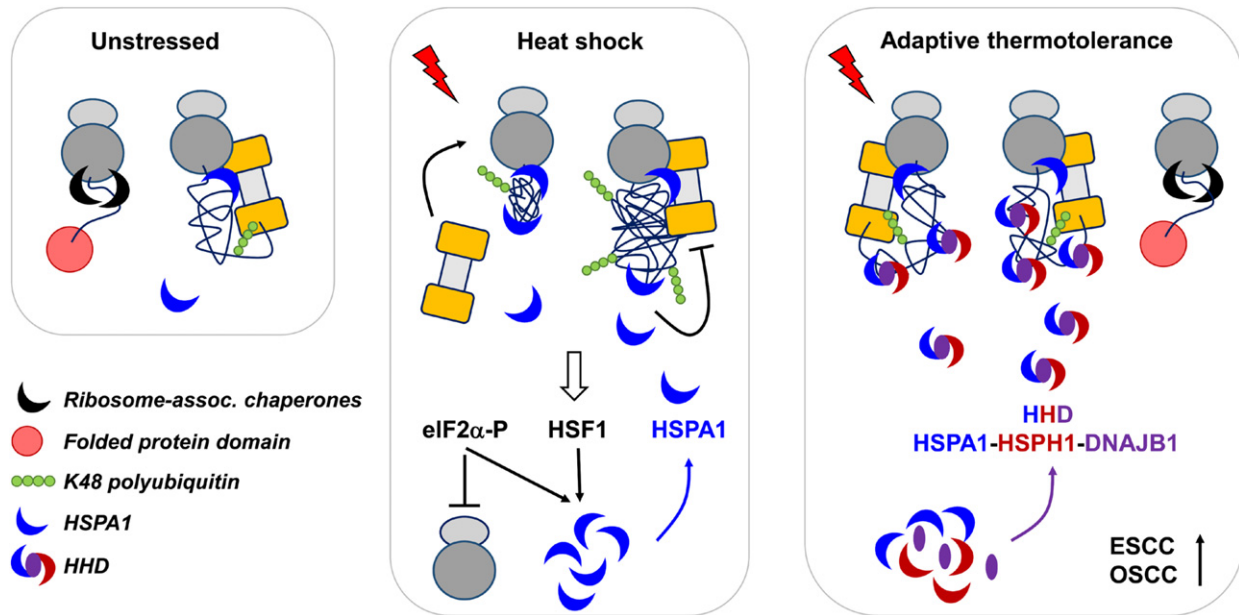


Figure 9. Model of the quality control of nascent/newly synthesized proteins and thermotolerance.

Under normal conditions (left panel), cells co-translationally fold newly synthesized proteins with high efficiency. A modest fraction of nascent peptides that cannot fold correctly will be ubiquitylated and targeted for degradation. Proteasomal targeting is aided by HSPA1, which is present in sufficient amounts to prevent the aggregation of damaged nascent peptides that would impede proteasomal clearance. In response to acute heat shock (middle panel), HSPA1 becomes limiting and aggregation of ubiquitylated nascent polypeptides impedes their degradation by the proteasome. Limitation in HSP70 activity leads to inhibition of global protein synthesis through phosphorylation of eIF2 α and mechanisms impinging on translation elongation. Simultaneously, activation of HSF1 leads to transcriptional induction and synthesis of HSPA1. In cells rendered thermotolerant through previous heat exposure and recovery (right panel), increased levels of HSPA1, HSPH1, and DNAJB1 provide increased activity of the HHD chaperone complex to facilitate rapid proteasomal clearance. As a result, eIF2 α phosphorylation subsides, and cells maintain protein synthesis despite the environmental challenge. Tumors, including esophageal and oral squamous carcinomas appear to gain a survival advantage by upregulating this pathway.

exposed to proteotoxic stress (Fig 7C) and in MCF7 cells treated with VER-155008 (Fig 2E).

A second key observation is that thermotolerant cells with increased HHD no longer respond to the primary insult—heat stress for 1 h—with accumulation of polyubiquitylated proteins in polysomes. In theory, this could be due to either (i) rapid refolding of damaged proteins thus preventing their ubiquitylation or (ii) rapid proteasomal degradation of polyubiquitylated polysomal proteins. Our data showing that polysomal polyubiquitylation is fully restored by treating heat-stressed MCF7^{4TT} cells with MG132 (Fig 5B) verifies the second scenario. The observations that VER-155008 (Fig 5B) and knockout of HSPH1 (Fig 7D) phenocopy MG132, substantiate an essential role of the HHD chaperone complex in the rapid degradation of nascent/newly synthesized proteins in thermotolerant cells re-challenged by acute heat stress. These results do not rule out an additional role for HHD in the refolding of heat-denatured proteins, although such refolding appears substantially slower in mammalian cells (Määttä *et al*, 2020) than in yeast (Wallace *et al*, 2015), and thus would not seem to occur on a time scale relevant to our observations.

Implications for cancer

Our results also assign a crucial role to HSPH1—and thus presumably HHD—in facilitating the proliferation of cancer

cells in tissue culture and in an animal host. Overexpression of HSPH1 has been found in multiple human cancers, including colon cancer, melanoma, and non-Hodgkin lymphoma (Chatterjee & Burns, 2017), whereas siRNA-mediated knock-down induces apoptosis of colon and gastric cancer cell lines (Hosaka *et al*, 2006). Likewise, we found strong overexpression of HSPH1 in digestive tract cancers with high prevalence in China (Fig 8B), and high levels of HSPH1 correlate with poor patient prognosis in these cancers (Fig 8C, Appendix Fig S6). These observations suggest a scenario in which high levels of HSPH1 would promote increased activity of the HHD complex that confers therapy resistance to oral and esophageal cancers. More generally, high HHD may allow a diverse set of cancers to adapt to the adverse conditions of the tumor microenvironment which is marked by a mutually reinforcing network of metabolic, genotoxic, and proteotoxic stresses (Luo *et al*, 2009; Gorrini *et al*, 2013). This may explain the sensitization of KYSE150^{HSPH1-/-} cells to combinations of stressors, including heat, MG132, and VER-155008. Significantly, the proposed role of HSPH1 in stress defense and its selective upregulation in diverse cancers nominate it as a target for therapeutic intervention. Indeed, first attempts at targeting HSPH1 suggest this as a promising avenue for future research (Gozzi *et al*, 2020).

Materials and Methods

Reagents and Tools table

Reagent/Resource	Reference or Source	Identifier or Catalog Number
Experimental Models		
Pathological section of oral squamous cell carcinoma	Department of Pathology, Chenggong Hospital of Xiamen University	
Pathological section of esophageal squamous cell carcinoma	Department of Pathology, Chenggong Hospital of Xiamen University	
BALB/c nu mice	Xiamen University Laboratory Animal Center	
MCF7 cell	Our Lab	
KYSE150 cell	Medical College of Shantou University	Provided by Dr. Guohong Zhang
Recombinant DNA		
<i>Indicate species for genes and proteins when appropriate</i>		
px459 VQR	Addgene	Cat #101715
Antibodies		
Rabbit Polyclonal Anti- RPL7 (WB 1:2,000)	Abcam	Cat# ab72550
Rabbit Polyclonal Anti- RPS19 (WB 1:2,000)	Bethyl	Cat# A304-002A
Rabbit Polyclonal Anti- HSP70/HSPA1 (WB 1:3,000)	Protein tech	Cat# 10995-1-AP
Rabbit Polyclonal Anti- HSP105/HSPH1 (WB 1:1,000)	Millipore	Cat# ABC264
Mouse Monoclonal Anti-Proteasome 20S/PSMA1-6 (WB 1:1,000)	Enzo	Cat# BML-PW8195
Rabbit Polyclonal Anti-PSMB1 (WB 1:1,000)	Protein tech	Cat# 11749-1-AP
Rabbit Polyclonal Anti-ADRM1 (WB 1:500)	Enzo	Cat# ENZ-ABS296
Rabbit Polyclonal Anti-PSMC1/Rpt2/S4 (WB 1:1,000)	Enzo	Cat# BML-PW0530
Rabbit Polyclonal Anti- DNAJC2/MP11 (WB 1:1,000)	Protein tech	Cat# 11971-1-AP
Rabbit Monoclonal Anti- K48-Linkage Polyubiquitin (WB 1:3,000)	Cell Signaling	Cat# 8081
Mouse Monoclonal anti- Puromycin (WB 1:3,000) (IP 5 µg/sample)	Millipore	Cat# Millipore-MABE343
Mouse Monoclonal anti- β-Actin (WB 1:2,000)	SIGMA-ALDRICH	Cat# A5441
Goat Anti-Rabbit IgG (WB 1:5,000)	Thermo	Cat# 31460
Goat Anti-Mouse IgG (WB 1:5,000)	Thermo	Cat# 31430
Oligonucleotides and other sequence-based reagents		
Crisper/Cas9 Guide RNA HSPH1-1F	CACCGTGAACCCGTTGTAACACAAC	
Crisper/Cas9 Guide RNA HSPH1-1R	AAACGTTGTGTTACAACGGGTTTCAC	
Crisper/Cas9 Guide RNA HSPH1-2F	CACCGCTCCACCATAGATGCCGTAG	
Crisper/Cas9 Guide RNA HSPH1-2R	AAACCTACGGCATCTATGGTGGAGC	
Crisper/Cas9 Guide RNA HSPH1-3F	CACCGAGATTGTTGGAGCGCTACA	
Crisper/Cas9 Guide RNA HSPH1-3R	AAACTGTAGCGCCTCCAACAATCTC	
Crisper/Cas9 Guide RNA HSPH1-4F	CACCGCACTCCTACGTCTGTATCA	

Reagents and Tools table (continued)

Reagent/Resource	Reference or Source	Identifier or Catalog Number
Crisper/Cas9 Guide RNA HSPH1-4R	AAACTGATACAGACGTAGGAGTGC	
U6F	ATGGACTATCATATGCTTACCGTA	
Chemicals, Enzymes and other reagents		
Recombinant Human His6-USP2 Catalytic Domain	Boston Biochem	Cat # E-506
Cycloheximide	Cell Signaling	Cat # 2112
MG132	MedChem Express	Cat # HY-13259
N-ethylmaleimide	BBI Life Sciences	Cat # A600450
Sodium deoxycholate	SIGMA-ALDRICH	Cat # 302-95-4
Triton X-100	SIGMA-ALDRICH	Cat # V900502-500ML
ATP	BBI Life Sciences	Cat # A600020
VER-155008	MedChem Express	Cat # HY-10941
Proteasome-Glo™ Assay (Chymotrypsin-Like Assay)	Promega	Cat # G8622
Proteasome-Glo™ Assay (Trypsin-Like Assay)	Promega	Cat # G8632
Proteasome-Glo™ Assay (Caspase-Like Assay)	Promega	Cat # G8642
Recombinant RNasin	Promega	Cat # N2511
Sure Beads™ Protein G Magnetic beads	BIO-RAD	Cat # 161-4023
SYPRO® Ruby Protein Gel Stain, 1 L	Invitrogen	Cat # S12000
Pierce protease inhibitor cocktail	MedChem Express	Cat # HY-K0011
Trypan blue	BIOSHARP	Cat # T-6146
IHC Kits	ZSGB-BIO	Cat # SPN-9001/2
DNA purification kit	TIANGEN	Cat # DP204-03
BCA Protein Assay Kit	TIANGEN	Cat # R6628
30%AcrylamidA/BisacrylA	LABLEAD	Cat # A3291
DMEM/high glucose	HyClone	Cat # SH30022.01
RPMI medium modified	HyClone	Cat # SH30809.01
Penicillin- streptomycin solution	HyClone	Cat # SV30010
Tris base	SIGMA-ALDRICH	Cat # V900483-5KG
Boric acid	Sangon Biotech	Cat # A500897-0005
HF-BbsI	NEB	Cat # R3539L
Rnase I	Invitrogen	Cat # AM2294
Urea	SIGMA-ALDRICH	Cat # U5218
7.5% PAGE Gel Fast Preparation Kit	EpiZyme	Cat # PG111
10% PAGE Gel Fast Preparation Kit	EpiZyme	Cat # PG112
Software		
GraphPad Prism 8	https://www.graphpad.com/scientific-software/prism/	
Image J	https://imagej.en.softonic.com/	
UV gradient profiling software	BIOCOMP	Version 7.73
Other		
Gradient master	BIOCOMP	108
Typhoon FLA 9500	GE	Version 1.0
Piston Gradient Fractionator	BIOCOMP	152
ChemiDoc™ imaging system	BIO-RAD	733BR2378
UV detector	BIO-RAD	ECONO UV MONITOR

Methods and Protocols

Cell culture

MCF7 cells were cultured in DMEM/High Glucose (HyClone, SH30022.01), 10% fetal bovine serum (FBS), 100 unit/ml penicillin, and 100 µg/ml streptomycin under 5% CO₂ at 37°C. KYSE150 cells were cultured in RPMI Medium Modified (HyClone, SH30809.01), 10% fetal bovine serum (FBS), 100 unit/ml penicillin, and 100 µg/ml streptomycin under 5% CO₂ at 37°C. Cells were authenticated by short tandem repeat sequencing and determined to be free of mycoplasma. For cell viability assays, trypan blue was added to the medium at a final concentration of 0.04% for 2 min. The media was replaced, and cells were qualitatively examined for staining by light microscopy. For quantification of cell viability, cells were trypsinized and counted in a counting chamber. Cell viability was calculated with the formula: %viability = trypan blue stained cells/(unstained cell + stained cells).

Proteotoxic stress

MCF7 and KYSE150 cells were plated in 6 cm dishes, grown to a density of ~80% and exposed to heat shock (42 or 45°C) followed by recovery (37°C) to induce heat stress response and thermotolerance. MG132 (Tocris, 1748) treatments were performed at 20 µM for 1 h, VER-155008 (Selleckchem, S7751) treatments were performed at 50 µM for 1 h.

Proteasome activity assay

5×10^6 cells were collected in ice-cold PBS. Pellets were resuspended in 0.45 ml hypotonic buffer (5 mM Tris-HCl, pH 7.5, 2.5 mM MgCl₂, 1.5 mM KCl and 1× Pierce™ protease inhibitor cocktail (MCE, HY-K0011), 1 mM DTT, 2 mM ATP). Cells were incubated in hypotonic buffer on ice for 10 min and vortexed for 15 s. Triton X-100 and sodium deoxycholate were added to final concentration of 0.5% each, and samples were vortexed for another 15 s. Cell lysates were centrifuged at 16,500 g for 8 min at 4°C. Supernatants (cytosolic cell extracts) were collected and proteasome activity was determined followed the descriptions provided with the kit (Promega, G8622).

Polysome profiling

100 µg/ml cycloheximide (CHX) was added to cells grown in 15 cm dishes 10 min prior to harvest. 5×10^7 cells were collected in 0.5 ml hypotonic buffer (5 mM Tris-HCl, pH 7.5, 2.5 mM MgCl₂, 1.5 mM KCl and 1× Pierce™ protease inhibitor cocktail) supplemented with 100 µg/ml CHX (Cell Signaling Technology 2112), 1 mM DTT, and 100 units of RNase inhibitor (Promega, N2111). Cells were incubated in hypotonic buffer on ice for 10 min and vortexed for 15 s. Triton X-100 and sodium deoxycholate were added to a final concentration of 0.5% each, and the total lysate were vortexed for another 15 s. The cell lysates were centrifuged at 16,500 g for 8 min at 4°C. Supernatants (cytosolic cell extracts) were collected and absorbance at OD 260 nm was measured. 20–30 OD₂₆₀ of lysate was gently layered over 10–50% cold sucrose gradients in buffer (20 mM HEPES-KOH, pH 7.4, 5 mM MgCl₂, 100 mM KCl, 100 µg/ml CHX, 10 units/ml RNase inhibitor and 1× Pierce™ protease inhibitor cocktail). To prepare the sucrose gradients, 50% sucrose solution (sucrose dissolved in gradient buffer) was layered below a 10% sucrose solution and solutions were mixed using the

Gradient Master 108 (Biocomp). Gradients were centrifuged at 220,000 g (Beckman, SW41Ti) for 2 h at 4°C. After centrifugation, the polysome profiles were recorded and fractionation through UV detector (BIO-RAD, ECONO UV MONITOR) and the Piston Gradient Fractionator (BIOCOMP, PGF).

For measurement of proteasome activity, 50 µl of each fraction were incubated with proteasome detection reagent (Promega, G8631). For immunoblotting, fractions were mixed with 40 µl 4× SDS sample buffer (200 mM Tris/Cl, pH 6.8, 5% beta-mercaptoethanol, 8% SDS, 40% glycerol, 0.4% bromophenol blue), followed by heating for 10 min at 95°C.

Digestion of polyubiquitin chains by recombinant USP2

Polysome containing lysate was collected as described above. To digest K48-polyubiquitin chains, the lysate was incubated with 7 µg of recombinant human USP2 catalytic domain protein (Boston Biochem, E-506) for 1 h at 25°C. After digest, the lysate was layered on top of a 10–50% cold sucrose gradient and subjected to density gradient centrifugation.

Puromycin release of nascent proteins

To release nascent proteins from ribosomes *in vivo*, 100 µg/ml puromycin was added into culture media for 10 min prior to collecting cells for lysate preparation and sucrose density gradient centrifugation.

SILAC sample preparation and quantitative proteomics

MCF7 cells were grown in DMEM containing heavy (¹³C, ¹⁵N) or light (¹²C, ¹⁴N) lysine and arginine supplemented with 5% dialyzed FBS for 2 weeks. Cells labeled with heavy amino acids were subjected to the heat shock and recovery treatments indicated in the figures. Control cells were maintained in standard (light) media. Cells were collected and lysed in RIPA buffer (50 mM Tris, 150 mM NaCl, 1% NP-40, 0.25% SDS, 1 mM EDTA, and 1× Pierce™ protease inhibitor cocktail). Protein concentrations were determined by BCA assay, and experimental samples (“heavy”) were mixed with the untreated control sample (“light”) at a ratio of 1:1. 200 µg of protein samples were applied for LC-MS/MS. Filter aided sample preparation (FASP) for LC-MS/MS was done as described (Wiśniewski *et al*, 2009). The digested peptide mixtures were re-dissolved in 0.1% formic acid in ultrapure water prior to LC-MS/MS, and the LC-MS/MS was performed as described (Lin *et al*, 2020). Protein identification and quantitation were performed by Thermo Proteome Discoverer (PD 2.1.1.2.) software against UniProt human protein database release 2016_09. Precursor ion mass tolerance was 10 ppm; fragment ion mass tolerance was 0.5 Da. The FDR of protein and peptide was 0.01. The mass spectrometry proteomics data have been deposited to the ProteomeXchange Consortium via the PRIDE partner repository (Perez-Riverol *et al*, 2019) with the dataset identifier PXD020140.

Differentially expressed proteins were defined as those proteins that were quantified based on replicate H/L ratios with a relative standard deviation of less than 30% (RSD < 0.3) and that differed from the mean with a Z factor > 1 or < -1. Enrichment of functional terms in the proteomic datasets was done with Metascape (Zhou *et al*, 2019). For each protein list, pathway and process enrichment analysis has been carried out with the following ontology sources:

GO Biological Processes and GO Cellular Components. The set of 5,491 human proteins detected in all combined proteomic analyses carried out was used as the enrichment background. Terms with a P value < 0.01 , a minimum count of 3, and an enrichment factor > 1.5 (the enrichment factor is the ratio between the observed counts and the counts expected by chance) were collected and grouped into clusters based on their membership similarities.

Proteasome purification

26S proteasomes were purified by two methods. Briefly, for method I (Guo *et al.*, 2015) plasmid pQCXIP-Rpn11-TBHA was stably transfected into AD293 cells. The cell lysate of AD293-Rpn11-TBHA stable transfected cell line was incubated with streptavidin beads, after washing steps the beads were collected and dissolved in 120 μ l 1 \times SDS sample buffer prior to immunoblotting. For method II (Besche *et al.*, 2009), the proteasome binding protein GST-UBL was expressed in *Escherichia coli* and purified. GST-UBL was incubated with proteasome containing cell lysate, followed by absorption to GSH-Sepharose beads. Beads were washed and eluted in 120 μ l 1 \times SDS sample buffer prior to immunoblotting.

Separation of soluble and insoluble proteins

5×10^6 cells were subjected to the treatments indicated in the figures, soluble and insoluble protein fractions were prepared by lysing cells in 500 μ l hypotonic buffer (supplemented with 20 μ M MG132, 50 μ M *N*-ethylmaleimide (NEM), 1 mM DTT, 1 \times PierceTM protease inhibitor cocktail, 2 mM ATP). Triton X-100 and sodium deoxycholate were added to the lysate to a final concentration of 0.5% each. 100 μ l of cell lysate was removed (total lysate), and the remainder was subjected to centrifugation at 20,000 g for 30 min. 120 μ l of supernatant (soluble fractions) was mixed with 40 μ l 4 \times SDS sample buffer, and pellets (insoluble fraction) were dissolved in 120 μ l 1 \times SDS sample buffer prior to immunoblotting.

Staining of protein gels with SYPRO Ruby

Protein samples were separated by SDS-PAGE, and gels were stained with SYPRO Ruby according to the protocol provided with the kit (Invitrogen, S12000). After fixation, staining, and washing, fluorescence signals were detected in a Typhoon FLA 9500 imaging system (GE) with the laser set to 473 nm.

Affinity purification of puromycylated nascent proteins

To label and release nascent peptides by puromycin, 1×10^7 cells were collected and washed with cold PBS, followed by lysis in 500 μ l of hypotonic buffer (supplemented with 20 μ M MG132, 50 μ M NEM, 1 mM DTT, 1 \times PierceTM protease inhibitor cocktail and 2 mM ATP) on ice for 1 h with vortexing for 10 s every 10 min. Lysates were clarified by centrifugation at 9,400 g for 1 min. 100 μ g/ml puromycin was added to the lysate, followed by incubation at room temperature for 1 h. 100 μ l of the supernatant were removed (total lysate). To pull down puromycylated proteins, anti-puromycin antibody (1:100) was added and incubated at 4 $^{\circ}$ C for 4 h. 50 μ l protein-G magnetic beads (BIO-RAD) blocked with 5% BSA and washed in lysis buffer twice were added, followed by overnight incubation. Beads were washed with 500 μ l of lysis buffer three times and resuspended in SDS sample buffer.

Sucrose cushion to enrich polysomal proteins

1×10^7 cells were subjected to the treatments indicated in the figures, and cell lysates were prepared as described for polysome profiling. 120 μ l of the lysate was mixed with 40 μ l 4 \times SDS sample buffer (total sample). 200 μ l of cell lysate was layered over a 1 ml cushion of 30% (V/W) sucrose (dissolved in 20 mM HEPES-KOH, pH 7.4, 5 mM MgCl₂, 100 mM KCl, 100 μ g/ml CHX and 1 \times PierceTM protease inhibitor cocktail). Samples were centrifuged at 110,000 g (Beckman, TLA-120.2) for 1 h at 4 $^{\circ}$ C. After centrifugation, pellets were digested with RNase I (5 μ l/sample) prior to 80S ribosome pull-down or resuspended in 160 μ l of 1 \times SDS sample buffer for SDS-PAGE. To separate soluble or insoluble ubiquitylated proteins present in polysomal fractions, 400 μ l lysis buffer supplement with 10 mM EDTA was used for resuspending pellets before separating the soluble and insoluble fractions by centrifugation as described above.

Native PAGE

5×10^6 cells were collected in ice-cold PBS and lysed in 200 μ l native lysis buffer (50 mM Tris-HCl, pH 7.4, 1 mM EDTA, 5 mM MgCl₂, 1 mM DTT, 2 mM ATP) by vortexing with glass beads (three times for 10 s) at 4 $^{\circ}$ C. After removal of the glass beads, extracts were cleared by centrifugation at 14,500 g for 10 min at 4 $^{\circ}$ C. Protein concentration was measured by monitoring OD₂₈₀ and mixed with 1/5 volume of 5 \times native loading buffer (250 mM Tris-HCl, pH 6.8, 50% Glycerol, 0.05% bromophenol blue). 20 μ g of each lysate was subjected to 4% native PAGE. Native gels were prepared as follows (recipe for one minigel): 2 ml 5 \times native buffer (0.45 M Tris base, 0.45 M boric acid, 10 mM MgCl₂, pH8.1–8.4), 1.34 ml 30% acrylamid/bisacrylamide, 0.5 ml glycerol, 6.08 ml H₂O, 1 mM ATP, 1 mM DTT, 80 μ l 10% APS, 8 μ l TEMED). Gels were left to polymerize at room temperature for 40 min. Gels were run at 75 V for 1 h and then at 125 V for 2 h in an ice bucket with pre-cold running buffer (0.09 M Tris base, 0.09 M boric acid, 2 mM MgCl₂, 1 mM ATP, 1 mM DTT).

Immunoblotting

For immunoblotting, samples were separated by SDS-PAGE or native PAGE and proteins were transferred onto a PVDF membrane. Membranes were blocked in 5% skim milk in TBST for 1 h at room temperature. Membranes were probed with primary and secondary antibodies as follows: RPL7 (Abcam, ab72550) 1:2,000, RPS19 (Bethyl, A304-002A) 1:2,000, Proteasome 20S/PSMA (Enzo, BML-PW8195) 1:1,000, ADRM1/RPN13 (Enzo, ENZ-ABS296) 1:500, PSMB1 (Proteintech, 11749-1-AP) 1:1,000, PSMC1/Rpt2/S4 (Enzo, BML-PW0530) 1:1,000, DNAJC2/MPP11 (Proteintech,11971-1-AP) 1:1,000, Anti-Puromycin (Millipore, MABE343) 1:3,000, Hsp70/HSPA1 (Proteintech, 10995-1-AP) 1:3,000, HSPH1 (Millipore-ABC264) 1:1,000, K48-Linkage-Specific Polyubiquitin (Cell Signaling, 8081) 1:3,000, Anti- β -Actin (SIGMA-ALDRICH, A5441) 1:2,000, Goat Anti-Mouse IgG (Thermo, 31430) 1:5,000, Goat Anti-Rabbit IgG (Thermo,31460) 1:5,000. All primary antibodies were diluted in 1% BSA in TBST, and blots were incubated overnight at 4 $^{\circ}$ C. Blots were washed with TBST (three times for 10 min). All secondary antibodies were diluted in 5% skim milk in TBST, and blots were incubated at room temperature for 1 h, followed by washing in TBST (three times for 10 min). Chemiluminescent detection reagent (Advansta, 191026-09) was added, and chemiluminescence signals were acquired by exposure to X-ray film. Blots that were used for quantifications were visualized with the ChemiDocTM imaging

system (BIO-RAD) in an exposure time accumulation approach, and the appropriate exposure signal were selected for quantification. Quantifications were performed using ImageJ software.

Quantification of signals across sucrose density gradients was performed as described above. The intensity in each fraction is displayed relative to the control, typically MCF7 at 37°C or sometimes thermoresistant MCF7^{ATT} cells at 42°C. Because the quantification is relative to the control, the value of the control in each fraction is exactly 1.0. If K-48 polyubiquitin (or proteasome activity in some instances) is increased in a gradient fraction under a given treatment, that will result in a relative increase of the signal and thus a value > 1.0.

Immunohistochemistry

Tissue sections from the archives of the Department of Pathology at the Chenggong Hospital of Xiamen University were stained with monoclonal antibodies (HSPH1, 1:50 for 2 h at room temperature; HSPA1, 1:200 for 2 h at room temperature) using the IHC kits (ZSGB-BIO, SPN-9001/2) according to the procedures provided by the manufacturer (ZSGB-BIO). Slides were scored by microscopy, according the staining result the protein expression levels were divided into negative (–, no staining of any tumor cells), weakly positive (+, faint or focal staining), moderately positive (++ , strong staining in a minority of cells), and strongly positive (+++ , strong signal in the majority of cells).

Knockout of HSPH1 using CRISPR-Cas9

To establish HSPH1 knock-out cell lines using the CRISPR-Cas9 system, guide RNAs (gRNAs) were designed using a web-based tool (<http://crispr.mit.edu/>). The vector plasmid px459 VQR was obtained from Addgene (#62988). Vector digest system: 1 µg px459 VQR was digested with HF-BbsI (NEB) and purified with a DNA purification kit (TIANGEN, DP204-03). The corresponding sense and antisense oligonucleotides listed below were annealed by incubation at 37°C for 30 min, heating to 95°C for 5 min, and cooling to 25°C at a rate of 5°C/min. Annealed oligos were ligated into px459 VQR and cloning products were confirmed by sequencing. To induce HSPH1 gene deletion, the plasmids were transfected into KYSE150 cells using Lipofectamine 2000 transfection reagent (Invitrogen) according to the procedures provided by the manufacturer. 48 h after transfection, cells were plated for the collection of individual clones. After 2 weeks, cell clones were tested for deletion of HSPH1 by immunoblotting.

gRNA used in this study:

oligo HSPH1-1F CACCGTGAACCCGTTGTAACACAAC
 oligo HSPH1-1R AAACGTTGTGTTACAACGGGTTCCAC
 oligo HSPH1-2F CACCGCTCCACCATAGATGCCGTAG
 oligo HSPH1-2R AAACCTACGGCATCTATGGTGGAGC
 oligo HSPH1-3F CACCGAGATTGTTGGAGGCGCTACA
 oligo HSPH1-3R AAACGTAGCGCCTCCAACAATCTC
 oligo HSPH1-4F CACCGCACTCCTACGTCTGTATCA
 oligo HSPH1-4R AAACGATACAGACGTAGGAGTGC

Tumor xenograft studies

BALB/c nude mice (5–6 weeks of age) were used for subcutaneous xenografts. Mice were maintained in a pathogen-free environment in a 12 h light/dark cycle at 40–60% humidity and 22–24°C with sterilized food and tap water ad libitum. 2.5×10^5 cells in a volume

of 100 µl were inoculated subcutaneously into nude mice. After tumor reached a diameter of ~ 3 mm, tumor sizes were monitored three times per week by measurement with a caliper and body weights were recorded. Tumor volumes were calculated according to the formula: volume = width² × length/2. Mice were sacrificed after three weeks and tumors were excised for analysis. For protein extraction, 100 µl tissue lysis buffer (50 mM Tris, 150 mM NaCl, 0.5 mM EDTA, 1 mM DTT, 1% Triton X-100, 0.5% sodium deoxycholate, 0.1% SDS and 1 mM PSMF) was added to 10 mg tumor tissue, followed by disruption with glass beads (three times for 10 s) at 4°C. Extracts were cleared by centrifugation at 12,000 g for 10 min at 4°C. 20 µl of the supernatant was diluted in 100 µl lysis buffer and 40 µl 4× SDS sample buffer for immunoblotting.

Quantification and statistical analysis

All *P* values were determined using the multiple t-tests function in GraphPad Prism 8 (two-stage linear step-up procedure of Benjamini, Krieger, and Yekutieli with *Q* set to 5%). Each row was analyzed individually, without assuming a consistent standard deviation.

Data availability

The mass spectrometry proteomics data have been deposited to the ProteomeXchange Consortium via the PRIDE partner repository (www.ebi.ac.uk/pride) (Perez-Riverol *et al.*, 2019) with the dataset identifier PXD025123 (<http://www.ebi.ac.uk/pride/archive/projects/PXD025123>).

Expanded View for this article is available online.

Acknowledgements

We wish to thank Alfred Goldberg and Xing Guo for plasmids. This work was funded through grants 81773771 and 31770813 from the National Science Foundation of China (D.A.W and W.D.), the Fujian Provincial Department of Science & Technology (2017J05138), and the Innovation Program of Xiamen University Department of Life Sciences & Human Health (Y.C). We thank R. Ding and the Mass Spectrometry Facility of the School of Pharmaceutical Sciences at Xiamen University for support. The support from the Equipment Platform of the State Key Laboratory of Cellular Stress Biology at Xiamen University is gratefully acknowledged.

Author contributions

Conceptualization, GT and DAW; Methodology, GT, CH, YY and WY; Formal analysis, GT, YC and WY; Investigation, GT, YY, CH and WY; Writing – original Draft, GT and DAW; Writing—review & editing, GT, YY, CH, WY, WD, YC and DAW; Visualization, GT, DAW; Supervision, WD, YC and DAW; Funding acquisition, WD, YC and DAW.

Conflict of interest

The authors declare that they have no conflict of interest.

References

- Amm I, Sommer T, Wolf DH (2014) Protein quality control and elimination of protein waste: The role of the ubiquitin–proteasome system. *Biochim Biophys Acta BBA Mol Cell Res* 1843: 182–196

- Bengtson MH, Joazeiro CAP (2010) Role of a ribosome-associated E3 ubiquitin ligase in protein quality control. *Nature* 467: 470–473
- Besche HC, Haas W, Gygi SP, Goldberg AL (2009) Isolation of mammalian 26S proteasomes and p97/VCP complexes using the ubiquitin-like domain from HHR23B reveals novel proteasome-associated proteins. *Biochemistry* 48: 2538–2549
- Besche HC, Sha Z, Kukushkin NV, Peth A, Hock E-M, Kim W, Gygi S, Gutierrez JA, Liao H, Dick L et al (2014) Autoubiquitination of the 26S proteasome on Rpn13 regulates breakdown of ubiquitin conjugates. *EMBO J* 33: 1159–1176
- Buchberger A, Bukau B, Sommer T (2010) Protein quality control in the cytosol and the endoplasmic reticulum: brothers in arms. *Mol Cell* 40: 238–252
- Chatterjee S, Burns TF (2017) Targeting heat shock proteins in cancer: a promising therapeutic approach. *Int J Mol Sci* 18: 1978
- Chuang SM, Chen L, Lambertson D, Anand M, Kinzy TG, Madura K (2005) Proteasome-mediated degradation of cotranslationally damaged proteins involves translation elongation factor 1A. *Mol Cell Biol* 25: 403
- Ciechanover A, Kwon YT (2017) Protein quality control by molecular chaperones in neurodegeneration. *Front Neurosci* 11: 185
- Döring K, Ahmed N, Riemer T, Suresh HG, Vainshtein Y, Habich M, Riemer J, Mayer MP, O'Brien EP, Kramer G et al (2017) Profiling Ssb-nascent chain interactions reveals principles of Hsp70-assisted folding. *Cell* 170: 298–311.e20
- Duttler S, Pechmann S, Frydman J (2013) Principles of cotranslational ubiquitination and quality control at the ribosome. *Mol Cell* 50: 379–393
- Faust O, Abayev-Avraham M, Wentink AS, Maurer M, Nillegoda NB, London N, Bukau B, Rosenzweig R (2020) HSP40 proteins use class-specific regulation to drive HSP70 functional diversity. *Nature* 587: 489–494
- Frydman J (2001) Folding of newly translated proteins in vivo: the role of molecular chaperones. *Annu Rev Biochem* 70: 603–647
- Gamerding M, Kobayashi K, Wallisch A, Kreft SG, Sailer C, Schlömer R, Sachs N, Jomaa A, Stengel F, Ban N et al (2019) Early scanning of nascent polypeptides inside the ribosomal tunnel by NAC. *Mol Cell* 75: 996–1006.e8
- Gorrini C, Harris IS, Mak TW (2013) Modulation of oxidative stress as an anticancer strategy. *Nat Rev Drug Discov* 12: 931–947
- Gozzi GJ, Gonzalez D, Boudesco C, Dias AMM, Gotthard G, Uyanik B, Dondaine L, Marcion G, Hermetet F, Denis C et al (2020) Selecting the first chemical molecule inhibitor of HSP110 for colorectal cancer therapy. *Cell Death Differ* 27: 117–129
- Guerrero C, Milenković T, Pržulj N, Kaiser P, Huang L (2008) Characterization of the proteasome interaction network using a QTAX-based tag-team strategy and protein interaction network analysis. *Proc Natl Acad Sci USA* 105: 13333–13338
- Guo X, Wang X, Wang Z, Banerjee S, Yang J, Huang L, Dixon JE (2015) Site-specific proteasome phosphorylation controls cell proliferation and tumorigenesis. *Nat Cell Biol* 18: 202–212
- Ha S-W, Ju D, Hao W, Xie Y (2016) Rapidly translated polypeptides are preferred substrates for cotranslational protein degradation. *J Biol Chem* 291: 9827–9834
- Hartl FU, Hayer-Hartl M (2009) Converging concepts of protein folding *in vitro* and *in vivo*. *Nat Struct Mol Biol* 16: 574–581
- Hartl FU, Bracher A, Hayer-Hartl M (2011) Molecular chaperones in protein folding and proteostasis. *Nature* 475: 324–332
- Higgins R, Gendron J, Rising L, Mak R, Webb K, Kaiser S, Zuzov N, Riviere P, Yang B, Fenech E et al (2015) The unfolded protein response triggers site-specific regulatory ubiquitylation of 40S ribosomal proteins. *Mol Cell* 59: 35–49
- Hjerpe R, Bett JS, Keuss MJ, Solovyova A, McWilliams TG, Johnson C, Sahu I, Varghese J, Wood N, Wightman M et al (2016) UBQLN2 mediates autophagy-independent protein aggregate clearance by the proteasome. *Cell* 166: 935–949
- Hosaka S, Nakatsura T, Tsukamoto H, Hatayama T, Baba H, Nishimura Y (2006) Synthetic small interfering RNA targeting heat shock protein 105 induces apoptosis of various cancer cells both *in vitro* and *in vivo*. *Cancer Sci* 97: 623–632
- Hundley HA, Walter W, Bairstow S, Craig EA (2005) Human Mpp11 J protein: ribosome-tethered molecular chaperones are ubiquitous. *Science* 308: 1032–1034
- Jaiswal H, Conz C, Otto H, Wolffe T, Fitzke E, Mayer MP, Rospert S (2011) The Chaperone network connected to human ribosome-associated complex. *Mol Cell Biol* 31: 1160–1173
- Joazeiro CAP (2019) Mechanisms and functions of ribosome-associated protein quality control. *Nat Rev Mol Cell Biol* 20: 368–383
- Kim W, Bennett E, Huttlin E, Guo A, Li J, Possemato A, Sowa M, Rad R, Rush J, Comb M et al (2011) Systematic and quantitative assessment of the ubiquitin-modified proteome. *Mol Cell* 44: 325–340
- Kramer G, Boehringer D, Ban N, Bukau B (2009) The ribosome as a platform for co-translational processing, folding and targeting of newly synthesized proteins. *Nat Struct Mol Biol* 16: 589–597
- Kramer G, Shiber A, Bukau B (2018) Mechanisms of cotranslational maturation of newly synthesized proteins. *Annu Rev Biochem* 88: 337–364
- Liao W, Yeung S-CJ, Chan L (1998) Proteasome-mediated degradation of apolipoprotein B targets both nascent peptides cotranslationally before translocation and full-length apolipoprotein B after translocation into the endoplasmic reticulum. *J Biol Chem* 273: 27225–27230
- Lin Y, Li F, Huang L, Polte C, Duan H, Fang J, Sun Li, Xing X, Tian G, Cheng Y et al (2020) eIF3 associates with 80S ribosomes to promote translation elongation, mitochondrial homeostasis, and muscle health. *Mol Cell* 79: 1–13
- Luo J, Solimini NL, Elledge SJ (2009) Principles of cancer therapy: oncogene and non-oncogene addiction. *Cell* 136: 823–837
- Määttä TA, Rettel M, Sridharan S, Helm D, Kurzawa N, Stein F, Savitski MM (2020) Aggregation and disaggregation features of the human proteome. *Mol Syst Biol* 16: e9500
- Medicherla B, Goldberg AL (2008) Heat shock and oxygen radicals stimulate ubiquitin-dependent degradation mainly of newly synthesized proteins. *J Cell Biol* 182: 663–673
- Mogk A, Bukau B, Kampina HH (2018) Cellular handling of protein aggregates by disaggregation machines. *Mol Cell* 69: 214–226
- Nagy Á, Lánckzy A, Menyhart O, Györfi B (2018) Validation of miRNA prognostic power in hepatocellular carcinoma using expression data of independent datasets. *Sci Rep* 8: 9227
- Nguyen AT, Prado MA, Schmidt PJ, Sendamarai AK, Wilson-Grady JT, Min M, Campagna DR, Tian G, Shi Y, Dederer V et al (2017) UBE2O remodels the proteome during terminal erythroid differentiation. *Science* 357: eaan0218
- Nillegoda NB, Kirstein J, Szlachcic A, Berynskyy M, Stank A, Stengel F, Arnsburg K, Gao X, Scior A, Aebersold R et al (2015) Crucial HSP70 co-chaperone complex unlocks metazoan protein disaggregation. *Nature* 524: 247–251
- Otto H, Conz C, Maier P, Wölffe T, Suzuki CK, Jenö P, Rücknagel P, Stahl J, Rospert S (2005) The chaperones MPP11 and Hsp70L1 form the mammalian ribosome-associated complex. *Proc Natl Acad Sci USA* 102: 10064–10069
- Pechmann S, Willmund F, Frydman J (2013) The ribosome as a Hub for protein quality control. *Mol Cell* 49: 411–421

- Perez-Riverol Y, Csordas A, Bai J, Bernal-Llinares M, Hewapathirana S, Kundu DJ, Inuganti A, Griss J, Mayer G, Eisenacher M *et al* (2019) The PRIDE database and related tools and resources in 2019: improving support for quantification data. *Nucleic Acids Res* 47: D442–D450
- Rico-Bautista E, Zhu W, Kitada S, Ganapathy S, Lau E, Krajewski S, Ramirez J, Bush JA, Yuan Z, Wolf DA (2013) Small molecule-induced mitochondrial disruption directs prostate cancer inhibition via UPR signaling. *Oncotarget* 4: 1212–1229
- Sato S, Ward CL, Kopito RR (1998) Cotranslational ubiquitination of cystic fibrosis transmembrane conductance regulator *in vitro*. *J Biol Chem* 273: 7189
- Schubert U, Antón LC, Gibbs J, Norbury CC, Yewdell JW, Bennink JR (2000) Rapid degradation of a large fraction of newly synthesized proteins by proteasomes. *Nature* 404: 770–774
- Sha Z, Brill LM, Cabrera R, Kleifeld O, Scheliga JS, Glickman MH, Chang EC, Wolf DA (2009) The eIF3 interactome reveals the translasome, a supercomplex linking protein synthesis and degradation machineries. *Mol Cell* 36: 141–152
- Shalgi R, Hurt JA, Krykbaeva I, Taipale M, Lindquist S, Burge CB (2013) Widespread regulation of translation by elongation pausing in heat shock. *Mol Cell* 49: 439–452
- Shiber A, Breuer W, Brandeis M, Ravid T (2013) Ubiquitin conjugation triggers misfolded protein sequestration into quality control foci when Hsp70 chaperone levels are limiting. *Mol Biol Cell* 24: 2076–2087
- Shiber A, Ravid T (2014) Chaperoning proteins for destruction: diverse roles of Hsp70 chaperones and their co-chaperones in targeting misfolded proteins to the proteasome. *Biomolecules* 4: 704–724
- Shorter J (2011) The mammalian disaggregase machinery: Hsp110 synergizes with Hsp70 and Hsp40 to catalyze protein disaggregation and reactivation in a cell-free system. *PLoS One* 6: e26319
- Stein KC, Kriel A, Frydman J (2019) Nascent polypeptide domain topology and elongation rate direct the cotranslational hierarchy of Hsp70 and TRiC/CCT. *Mol Cell* 75: 1117–1130.e5
- Stolz A, Wolf DH (2010) Endoplasmic reticulum associated protein degradation: a chaperone assisted journey to hell. *Biochim Biophys Acta BBA - Mol Cell Res* 1803: 694–705
- Sugiyama T, Li S, Kato M, Ikeuchi K, Ichimura A, Matsuo Y, Inada T (2019) Sequential ubiquitination of ribosomal protein uS3 triggers the degradation of non-functional 18S rRNA. *Cell Rep* 26: 3400–3415.e7
- Thommen M, Holtkamp W, Rodnina MV (2017) Co-translational protein folding: progress and methods. *Curr Opin Struct Biol* 42: 83–89
- Turner GC, Varshavsky A (2000) Detecting and measuring cotranslational protein degradation *in vivo*. *Science* 289: 2117–2120
- Wallace E, Kear-Scott J, Pilipenko E, Schwartz M, Laskowski P, Rojek A, Katanski C, Riback J, Dion M, Franks A *et al* (2015) Reversible, specific, active aggregates of endogenous proteins assemble upon heat stress. *Cell* 162: 1286–1298
- Wang Q, Liu Y, Soetandyo N, Baek K, Hegde R, Ye Y (2011) A Ubiquitin ligase-associated chaperone holdase maintains polypeptides in soluble states for proteasome degradation. *Mol Cell* 42: 758–770
- Wang F, Durfee LA, Huijbregtse JM (2013) A cotranslational ubiquitination pathway for quality control of misfolded proteins. *Mol Cell* 50: 368–378
- Wang F, Canadeo LA, Huijbregtse JM (2015a) Ubiquitination of newly synthesized proteins at the ribosome. *Biochimie* 114: 127–133
- Wang L, Delahunty C, Fritz-Wolf K, Rahlfs S, Prieto JH, Yates JR, Becker K (2015b) Characterization of the 26S proteasome network in *Plasmodium falciparum*. *Sci Rep* 5: 17818
- Wentink AS, Nillegoda NB, Feufel J, Ubartaitė G, Schneider CP, De Los Rios P, Hennig J, Barducci A, Bukau B (2020) Molecular dissection of amyloid disaggregation by human HSP70. *Nature* 587: 483–488
- Willmund F, del Alamo M, Pechmann S, Chen T, Albanèse V, Dammer EB, Peng J, Frydman J (2013) The cotranslational function of ribosome-associated Hsp70 in eukaryotic protein homeostasis. *Cell* 152: 196–209
- Wiśniewski JR, Zougman A, Nagaraj N, Mann M (2009) Universal sample preparation method for proteome analysis. *Nat Methods* 6: 359–362
- Yau RG, Doerner K, Castellanos ER, Haakonsen DL, Werner A, Wang N, Yang XW, Martinez-Martin N, Matsumoto ML, Dixit VM *et al* (2017) Assembly and function of heterotypic ubiquitin chains in cell-cycle and protein quality control. *Cell* 171: 918–933.e20
- Zhou Y, Zhou B, Pache L, Chang M, Khodabakhshi AH, Tanaseichuk O, Benner C, Chanda SK (2019) Metascape provides a biologist-oriented resource for the analysis of systems-level datasets. *Nat Commun* 10: 1523



License: This is an open access article under the terms of the Creative Commons Attribution-NonCommercial-NoDerivs 4.0 License, which permits use and distribution in any medium, provided the original work is properly cited, the use is non-commercial and no modifications or adaptations are made.